Available online at www.CivileJournal.org

Civil Engineering Journal

(E-ISSN: 2476-3055; ISSN: 2676-6957)

Vol. 12, No. 05, May, 2026

Waterproofing Admixture and Aloe Vera Biopolymer Gel in Concrete: Microstructure, Durability and Structural Validation

Marlon Cubas [1*], Pedro Patazca [1], Robert Suclupe [1], Luis Villegas [1], Omar Coronado [2], Oscar Alvarado [1], Javier Guerrero [1], Brayan Perleche [1]

[1] *Department of Civil Engineering, Faculty of Engineering and Architecture, César Vallejo University, Chiclayo 14012, Peru.*

[2] *School of Civil Engineering, Faculty of Civil, Systems, and Architecture Engineering (FICSA), National University Pedro Ruiz Gallo, Lambayeque 14013, Peru.*

Received 09 February 2026; Revised 19 April 2026; Accepted 22 April 2026; Published 01 May 2026

Abstract

Concrete durability in aggressive environments is often limited by chloride ingress, carbonation, and sulfate attack, which compromise structural integrity and increase maintenance costs. This study examines the combined effects of an integral waterproofing admixture (Sika®-1, 3– 4% cement weight) and Aloe vera biopolymer (1–2% cement weight) on mechanical performance, durability, and microstructural characteristics of conventional concrete. Four mixtures were produced: a control (P1) and three hybrid formulations (P2: 4%S1+1%AV; P3: 3.5%S1+1.5%AV; P4: 3%S1+2%AV), subjected to fresh state testing, strength development at 7, 14, and 28 days, and durability assessment including water permeability, chloride penetration, sulfate resistance, carbonation depth, ultrasonic pulse velocity, and surface abrasion through 56 days, alongside X-ray diffraction, Fourier-transform infrared spectroscopy, and scanning electron microscopy analysis. The optimal mixture (P4) achieved 28.77 MPa compressive strength, reduced water permeability to 0.00420 cm/s, lowered chloride penetration to 138.38 Coulombs, and minimized carbonation depth to 0.44 mm, with microstructural analysis revealing enhanced C-S-H gel densification and refined porosity. Pilot-scale reinforced concrete frames fabricated with P4 exhibited 9.6% lower maximum strain, confirming improved structural stiffness and durability. Techno-economic evaluation yielded an index of 1.104, demonstrating economic viability despite an 11.2% material cost increase. These results support the use of the hybrid admixture system as a sustainable option for extending concrete service life in marine, industrial, and tropical environments.

Keywords: Waterproofing Admixture; Aloe Vera Biopolymer; Concrete Durability; Chloride Permeability; Sustainable Construction.

1. Introduction

Concrete durability represents a critical determinant of infrastructure service life, economic viability, and environmental sustainability [1]. Structures subjected to aggressive environmental conditions (including chloride penetration, carbonation, sulfate attack, and freeze-thaw cycles) experience accelerated deterioration that compromises structural integrity and increases life-cycle costs [2, 3]. Recent analyses indicate that extending concrete service life through enhanced durability can reduce maintenance expenditures by up to 50% over the structure's lifespan, while simultaneously decreasing the environmental footprint associated with repair materials and reconstruction activities [4-6]. The use of advanced admixtures and supplementary materials is now a key strategy to improve concrete performance, helping structures withstand harsh conditions while also meeting sustainability targets [7-10].

* Corresponding author: carmasmar@ucvvirtual.edu.pe

https://doi.org/10.28991/CEJ-2026-012-05-09

Integral waterproofing admixtures have gained widespread adoption as effective solutions for mitigating water ingress and enhancing concrete impermeability. These chemical additives, typically silicate-based or crystalline compounds, modify the pore structure of the cementitious matrix by blocking capillary pathways and promoting secondary crystallization within microcracks. Research demonstrates that crystalline waterproofing admixtures can reduce water penetration depth and exhibit self-healing and pore-sealing effects that improve the durability of cement-based materials. Furthermore, these admixtures have been shown to improve resistance to chloride ion penetration and reduce permeability under pressure, thereby extending the effective service life of concrete structures exposed to marine and industrial environments [11-14].

Recent quantitative evaluations corroborate these trends. Suwondo et al. [15] reported that crystalline waterproofing admixture (CWA) at 1% and 2% by weight of cement reduced water penetration depth by 53% and 65%, respectively, while improving compressive strength by 5.4–6.1%. Wang et al. [16] demonstrated via SEM that CWA at 2% produced the densest C-S-H (calcium silicate hydrate) morphology and optimal pore refinement in concrete with a water-to-binder ratio of 0.45. These studies establish the individual performance envelope of crystalline waterproofing agents, against which hybrid formulations must be evaluated.

It is necessary at this point to distinguish between two classes of admixture that are often conflated in the literature. Synthetic superplasticizers disperse cement particles during mixing through the combined action of electrostatic repulsion from adsorbed carboxylate groups and steric hindrance from polyethylene glycol side chains; they reduce water demand and improve workability, but they do not intrinsically generate pore-blocking phases in the hardened matrix [17, 18]. By contrast, integral waterproofing admixtures are typically based on colloidal silicates or crystalline compounds that react in the presence of moisture and calcium-bearing phases within the pore network, promoting secondary crystallization and additional C-S-H formation that densify the matrix and obstruct fluid transport pathways [19]. Recent studies have clarified the distinct mechanisms governing these admixture classes. Wang et al. [16] and Fang et al. [17] showed that polycarboxylate superplasticizers modify the rheological behavior of cement slurries primarily through adsorption-driven dispersion and steric hindrance effects, improving fluidity without generating pore-blocking products in the hardened matrix. By contrast, studies on crystalline waterproofing admixtures, including those by Gojević et al. [20], have shown that moisture-activated secondary crystallization can densify the cementitious microstructure and promote crack sealing or self-healing behavior in small capillary fissures, a function that conventional superplasticizer-only systems do not provide. These mechanistic differences further strengthen the rationale for combining a pore-blocking waterproofing agent with a bio-based admixture capable of internal curing and hydration-product nucleation [21-23].

Table 1 summarizes these differences and, for comparison, also includes the mechanisms attributed to biopolymer gels. Recognizing this distinction is essential for understanding the hypothesis tested in the present study: Sika-1 acts primarily by refining and blocking residual capillary pathways in the hardened matrix, whereas Aloe vera gel acts across both the fresh and hardened states by retaining water during hydration, modifying rheology, and promoting denser hydration products through calcium-polysaccharide interactions [24, 25]. Because these two agents operate at different stages of cement hydration and at different scales of pore refinement, complementary rather than redundant effects may be expected; however, this specific combination has not yet been validated comprehensively through an integrated microstructural, durability, and structural assessment [9].

Table 1. Mechanistic comparison of admixture types used in concrete modification

Feature	Synthetic superplasticizer (PCE)	Integral waterproofing admixture	Biopolymer gel (Aloe vera)	References
Active chemistry	Colloidal sodium silicate / $CaCl_2$ backbone with grafted PEG side chains	Colloidal sodium silicate blended with $CaCl_2$ as accelerator	Acemannan-rich polysaccharide network extracted from *A. barbadensis* parenchyma	[17, 18]
How it works	Carboxylate groups adsorb onto cement grains and build up negative surface charge; the PEG side chains then keep particles apart through steric repulsion, freeing trapped water	Silicate ions react with $Ca(OH)_2$ during hydration and precipitate needle-like crystals inside capillary pores; these deposits grow further whenever moisture re-enters the matrix	Polysaccharides hold mixing water near unhydrated grains, extending internal curing; Ca^{2+} –polysaccharide complexes also serve as extra nucleation sites for C-S-H	[17, 26]
When it acts	Fresh state only (mixing and placing)	Hardened state, moisture-activated over time	Both stages; modifies rheology when fresh, promotes densification as concrete cures	[26, 27]
Effect on pore network	Indirect: lower effective w/c yields a tighter paste, but no crystals form	Direct: needle-shaped precipitates physically seal capillary channels; cracks up to ≈0.4 mm can re-heal	Direct: denser C-S-H around aggregates and a narrower pore-size distribution in the ITZ	[28, 29]
Durability contribution	Strength gain via water reduction (20–40%); no autonomous permeability benefit	Cuts water penetration 43–65%; lowers chloride ingress; improves sulfate resistance	Reduces carbonation depth; improves abrasion and chloride resistance at the right dosage	[12, 30, 31]
Practical limitation	Does not block pores on its own; no self-healing capacity	Overdosing can produce a non-structural gel layer; does not improve fresh-state workability	Batch-to-batch variability in gel composition; shelf-life sensitivity; possible set retardation above ≈2% bwoc	[32-34]

A bibliometric review by Kalokhe et al. [9] spanning publications from 2014 to 2024 identified cellulose, chitosan, and plant-derived gels as the most actively investigated sustainable admixtures for concrete, yet observed that fewer than 5% of the studies reviewed combined biopolymers with inorganic waterproofing agents. Vignesh et al. [11] further

confirmed that biopolymer-integrated concrete enhances long-term structural reliability through microstructural densification, but stressed that multi-scale validation connecting SEM/FTIR evidence with durability metrics and structural-scale testing remains scarce. Separately, Oshim et al. [13] developed a regression model for aloe vera gel concrete and identified 2.0% by weight of cement as the optimum dosage for compressive strength, yielding 31.42 MPa at 28 days.

Despite extensive research on integral waterproofing admixtures and biopolymer gels as separate additions, evidence on their combined use is still limited, particularly when linking microstructural changes to durability and structural performance. Most hybrid-additive studies report strength and a small set of durability indicators, but rarely integrate (i) microstructural characterization, (ii) pilot-scale structural testing under realistic loading, and (iii) a techno-economic check within the same experimental program. In this study, we evaluate three Sika-1/Aloe vera hybrid dosages (4S1–1AV, 3.5S1–1.5AV, and 3S1–2AV) and assess fresh properties, strength, durability/transport indicators, and microstructure, followed by pilot-scale reinforced concrete frame validation of the optimal mixture. The selected mixture (P4) achieves low permeability, low RCPT charge passed, shallow carbonation depth, improved structural stiffness, and a cost–benefit index of 1.104. Novel contribution: This work provides, to the best of the authors' knowledge, the first integrated multi-scale validation of a colloidal silicate waterproofing admixture combined with Aloe vera biopolymer gel, linking XRD/FTIR/SEM microstructural evidence to transport-based durability metrics, pilot-scale structural response, and a cost–benefit index within a single experimental program.

Primary hypothesis: The combination of Sika®-1 (3–4% bwoc) with Aloe vera biopolymer gel (1–2% bwoc) generates complementary pore-refinement mechanisms, crystalline precipitation in macrocapillaries and polysaccharide-mediated C-S-H nucleation in mesopores, that reduce water permeability and chloride ion transport below the levels achievable by either admixture alone, while maintaining or improving 28-day compressive strength relative to the control mixture. Secondary hypotheses. (i) The biopolymer's water-retention capacity improves fresh-state workability and early-age hydration kinetics without exceeding ASTM C143 slump limits; (ii) the hybrid system reduces carbonation depth through densified C-S-H gel formation that limits CO_2 diffusion; (iii) microstructural changes detectable by XRD, FTIR, and SEM provide mechanistic evidence for the observed macroscopic performance differences; and (iv) the optimal formulation maintains economic viability as quantified by a cost–benefit index $G_i \geq 1.0$.

The primary objective of this research is to comprehensively evaluate the performance of concrete incorporating integral waterproofing admixture (Sika®-1) and Aloe vera biopolymer gel through a multi-scale experimental program encompassing fresh properties, mechanical strength development, durability performance, microstructural analysis, structural validation, and cost–benefit assessment. The specific contributions of this work include:

- Investigation of three hybrid dosages (4%S1+1%AV, 3.5%S1+1.5%AV, 3%S1+2%AV) compared to control concrete across 7, 14, 28, and 56-day curing periods;
- Durability evaluation including water permeability, rapid chloride permeability (ASTM C1202), sulfate resistance (ASTM C1012), carbonation depth, ultrasonic pulse velocity (ASTM C597), and surface abrasion (ASTM C944);
- Microstructural characterization via X-ray diffraction (XRD), Fourier-transform infrared spectroscopy (FTIR), and scanning electron microscopy (SEM) to elucidate phase composition, functional group interactions, and morphological changes in the optimal mixture relative to control concrete;
- Pilot-scale structural validation through testing of reinforced concrete frames under vertical and horizontal loading conditions to assess real-world performance, load-displacement behavior, cracking patterns, and failure modes;
- Techno-economic analysis employing a cost–benefit index methodology adapted from Yu et al. [35] to quantify the economic viability of the optimal mixture considering material costs and performance gains.

2. Materials and Methods

2.1. Materials

Figure 1 summarizes the methodological framework of this study as an integrated eight-phase workflow designed to evaluate the hybrid concrete system from constituent characterization to structural and techno-economic validation. The program began with the selection and physicochemical characterization of cement, aggregates, Sika®-1, and Aloe vera gel, followed by mixture proportioning for the control concrete and three hybrid formulations. Subsequent phases comprised concrete production, fresh-state testing, and specimen fabrication; mechanical testing at 7, 14, and 28 days; and durability assessment through 56 days, including water permeability, rapid chloride permeability, sulfate resistance, carbonation depth, ultrasonic pulse velocity, and surface abrasion. The workflow was then extended to microstructural characterization by XRD, FTIR, and SEM, pilot-scale structural validation using reinforced concrete frames, and a final techno-economic appraisal based on a cost-benefit index. The following subsections present each methodological stage in the sequence shown in Figure 1.

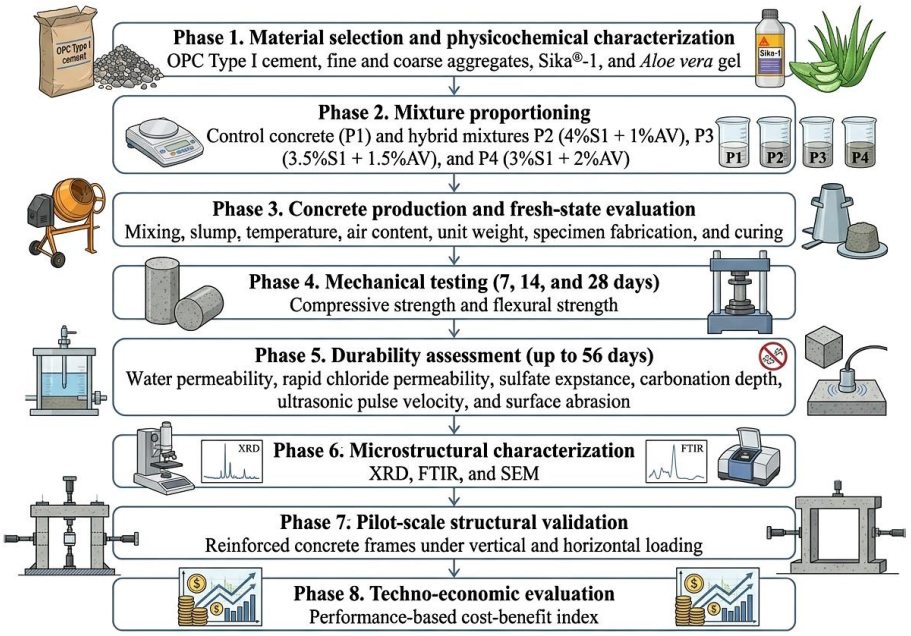

Figure 1. Experimental methodology workflow

2.1.1. Cement and Aggregates

Ordinary Portland Cement (OPC) Type I conforming to Peruvian standard NTP 334.009 and ASTM C150 was utilized. The cement was supplied by Cementos Pacasmayo (Trujillo, Peru), and exhibited the following chemical composition: CaO = 63.15%, SiO_2 = 20.84%, Al_2O_3 = 5.48%, Fe_2O_3 = 2.42%, SO_3 = 2.64%, MgO = 1.92%, Na_2O equivalent = 0.64%, and loss on ignition (LOI) = 3.10%. Physical properties included a specific gravity of 3.14 g/cm³, Blaine fineness of 3,450 cm²/g, initial and final setting times of 135 min and 280 min, respectively, determined according to NTP 334.009. The granulation of the aggregates used is shown in Figure 2.

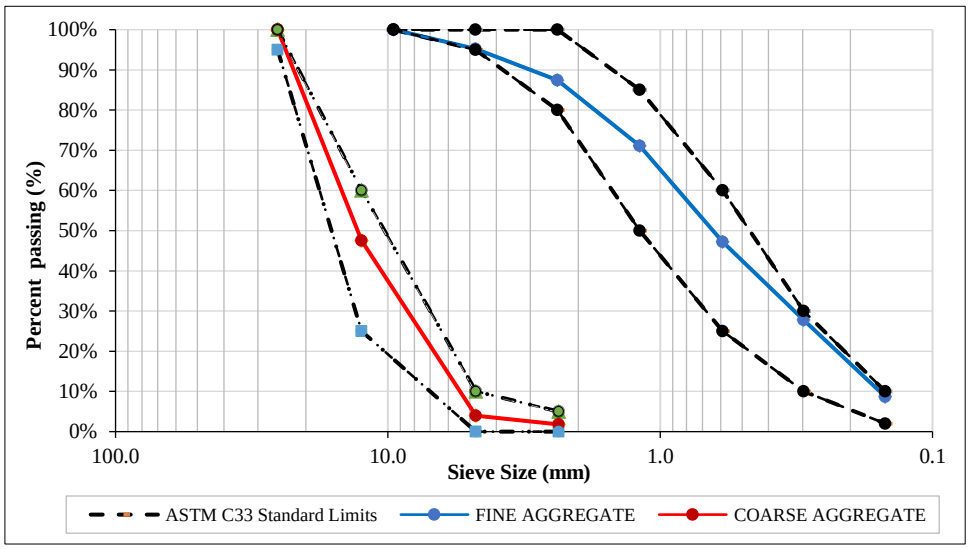

Figure 2. Particle size distribution of the aggregates used in concrete

2.1.2. Integral Waterproofing Admixture (S1)

The integral waterproofing admixture employed was Sika®-1 Integral Waterproofing Agent (Sika Perú S.A.C., origin: Sika, Switzerland), classified as a colloidal silicate emulsion designed for incorporation into the concrete matrix during mixing. The chemical composition, according to the product safety data sheet, comprises sodium silicate (5–10% by mass, CAS 1344-09-8), calcium chloride (5–10% by mass, CAS 10043-52-4) as a hydration accelerator and densifying agent, and water/dispersant matrix (80–90% by mass). The admixture exhibited a density of approximately 1.0 g/cm³, pH of 9.5–10.0 (10% aqueous dilution), and an estimated solid content of 15–25% based on the composition declaration. The mechanism of action involves blockage of capillary pores and reaction of colloidal silicates with cement during hydration, forming mineral precipitates that obstruct the capillary network and enhance water impermeability.

The product is classified as chloride-free ($Cl^- \leq 0.1\%$ by mass) and free of hazardous organic components, with a recommended dosage of approximately 3% by weight of cement (bwoc) as supplied by the manufacturer.

2.1.3. Aloe vera Biopolymer Gel Preparation

The biopolymer additive was fresh gel extracted from *Aloe barbadensis Miller* (commonly known as Aloe vera) sourced from cultivated plants in Lambayeque, Chiclayo, Peru. Mature leaves (2–2.5 years old, length ≥ 50 cm, basal thickness > 2.5 cm) were harvested and manually peeled using a sharp knife, with complete removal of the outer green epidermis and the yellow aloin layer. The gel was extracted by mechanical blending (liquidizer at 10,000 rpm) and passed through a stainless-steel mesh (aperture ca. 1 mm) to remove coarse fibers and cellular material. The resulting liquid gel was refrigerated at 4–5°C and used within 24–48 hours of preparation to preserve polysaccharide integrity and prevent microbial degradation. No chemical preservatives or stabilizers were added. The fresh gel exhibited the following physicochemical properties: pH = 9.5, density = 1.030 g/cm³, solids content = 1,030 mg/L (approximately 0.1% by mass), and dynamic viscosity ≈ 450 cP at 20°C. These properties are consistent with the water-soluble polysaccharide matrix (primarily arabinose, glucose, and mannose derivatives) and minor protein/amino acid components characteristic of AV parenchymal tissue. The extraction and preparation steps are illustrated in Figure 3.

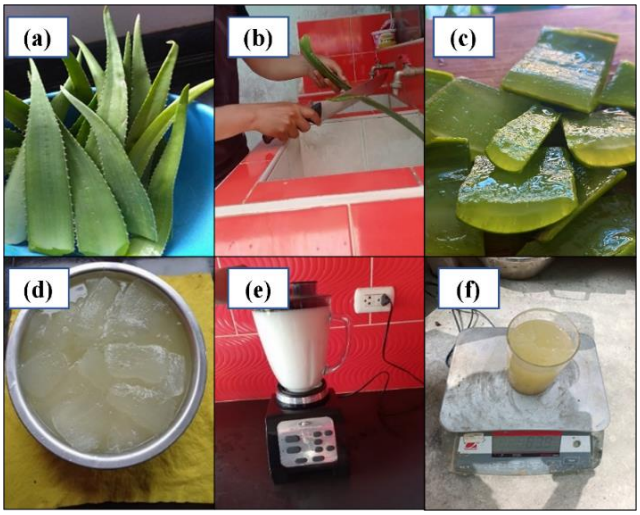

Figure 3. AV gel extraction process

The primary bioactive polysaccharide in *Aloe barbadensis Miller* gel is acemannan, an acetylated β-(1→4)-linked glucomannan with a molecular weight of approximately 200 kDa, characterized by acetyl groups at positions O-2, O-3, and O-6 of the mannose backbone, with galactose and arabinose side chains [19, 36]. Acemannan concentration varies with season: Aranda Cuevas et al. [37] quantified 99.97 ppm during the rainy season versus 106.03 ppm during the dry season in the high-molecular-weight fraction, with a more pronounced variation (9.36 vs. 26.94 ppm) in the low-molecular-weight fraction [34]. Plant age also influences polysaccharide yield; three-year-old specimens contain the highest acemannan content relative to two- and four-year-old plants. Processing conditions, particularly drying and thermal exposure, can reduce acemannan yield by approximately 40% and significantly alter its functional properties [34]. In the present study, all gel was harvested from plants aged 2–2.5 years during the same season (austral winter, Lambayeque, Peru) and processed within 24–48 hours without drying or preservatives to minimize batch-to-batch variability. However, direct quantification of acemannan content was not performed, which constitutes a limitation. Future studies should incorporate HPLC or ^{1}H-NMR characterization to enable reproducible standardization of the biopolymer dosage [25].

2.2. Mixture Proportions and Specimen Preparation

2.2.1. Mixture Design

A reference concrete mixture (P1, control) was designed using the ACI 211.1 method targeting a nominal compressive strength of 21 MPa at 28 days. The control mixture exhibited a water-to-cement ratio (w/c) of 0.56, cement content of 363 kg/m³, effective water content of 205 l/m³, fine aggregate content of 808 kg/m³, and coarse aggregate content of 937 kg/m³, yielding a calculated fresh unit weight of 2,313 kg/m³. The target slump was approximately 100 mm (4 inches), with an estimated air content of 2%.

The dosage ranges for Sika-1 and Aloe vera gel were selected on the basis of three criteria: (i) the manufacturer's recommended dosage for Sika-1 is approximately 3% bwoc, and the upper limit of 4% represents a 33% overdose intended to probe boundary effects on workability and pore structure; (ii) prior experimental studies have consistently

identified 2.0–2.5% bwoc as the optimal Aloe vera dosage for compressive strength improvement, establishing 2.0% as the practical upper bound; and (iii) preliminary trial batches (data not reported herein) confirmed that Aloe vera dosages exceeding 2.5% bwoc caused excessive set retardation (initial setting time >300 min), rendering the mixtures impractical for field placement. The three experimental combinations maintain a roughly constant total admixture content of approximately 5.0% bwoc while progressively shifting the proportion from waterproofing-dominant (P2: 4%S1+1%AV) to biopolymer-dominant (P4:3%S1+2%AV), enabling systematic assessment of each component's contribution [24, 26, 38].

Three experimental mixtures (P2, P3, P4) were prepared by incorporating the integral waterproofing admixture (S1) and Aloe vera biopolymer gel (AV) at the following dosages, expressed as percentages by weight of cement (bwoc):

- P2: 4.0% S1 + 1.0% AV (equivalent to 14.52 kg/m³ S1 and 3.63 kg/m³ AV);
- P3: 3.5% S1 + 1.5% AV (equivalent to 12.71 kg/m³ S1 and 5.45 kg/m³ AV);
- P4: 3.0% S1 + 2.0% AV (equivalent to 10.89 kg/m³ S1 and 7.26 kg/m³ AV).

The water content in experimental mixtures was adjusted by subtracting the liquid contribution of S1 and AV from the base water requirement to maintain an effective w/c ratio of 0.56, ensuring comparability with the control mixture. The liquid contributions were calculated as follows: S1 solids content (20% estimated) reduced the effective liquid requirement by 80% of the admixture mass, and AV (0.1% solids) was treated as 99.9% water.

2.2.2. Mixing Procedure

Concrete was produced using a rotary drum mixer with a capacity of 0.028 m³. The mixing sequence employed was as follows: (1) coarse aggregate and one-third of the design water were introduced; (2) fine aggregate and one-third of the design water were added; (3) cement and the remaining water (previously combined with S1 and AV for experimental mixtures) were introduced. The admixtures (S1 and AV) were pre-blended with the mixing water for 5 minutes at 10,000 rpm using a mechanical blender to ensure uniform dispersion prior to addition to the mixer. Total mixing time was 6 minutes, and no delay occurred between mixing completion and specimen casting. Mixing was conducted at ambient temperature (22 ± 2°C) in compliance with ASTM C192.

2.2.3. Specimen Preparation and Curing

Concrete was cast into three types of molds conforming to ASTM C192 and Peruvian standard NTP 339.183: (i) cylindrical specimens for compressive strength testing (diameter 150 mm × height 300 mm); (ii) prismatic beam specimens for flexural strength testing (150 mm × 150 mm × 550 mm); and (iii) smaller prismatic specimens for durability testing (100 mm × 100 mm × 500 mm). All specimens were compacted by rodding (25 strokes per layer, 2 layers) immediately after placing. Specimens were demolded 24 hours after casting and then submerged in saturated lime water at 23 ± 2°C and relative humidity > 95% until the time of testing. The casting and curing procedures for the different specimen types are shown in Figure 4.

Figure 4. Specimen preparation and curing process

The experimental program included testing at 7, 14, 28, and 56 days (where applicable). The number of specimens per test, age, and mixture is summarized in Table 2.

Table 2. Number of specimens per test, age and mixture

Mix	Age	Compressive strength	Flexural strength	Permeability (k)	Carbonation	Concrete abrasion	Chloride ion penetration	Sulfate expansion	Ultrasonic pulse velocity
P1	7	3	3	-	-	-	-	3	-
	14	3	3	-	-	-	-	3	-
	28	3	3	-	3	3	3	3	3
	56	-	-	3	3	3	3	3	3
P2	7	3	3	-	-	-	-	-	-
	14	3	3	-	-	-	-	-	-
	28	3	3	-	3	-	-	-	-
	56	-	-	3	3	-	-	-	-
P3	7	3	3	-	-	-	-	-	-
	14	3	3	-	-	-	-	-	-
	28	3	3	-	3	-	-	-	-
	56	-	-	3	3	-	-	-	-
P4	7	3	3	-	-	-	-	3	-
	14	3	3	-	-	-	-	3	-
	28	3	3	-	3	3	3	3	3
	56	-	-	3	3	3	3	3	3

2.3. Fresh Concrete Testing

Fresh concrete properties were determined according to ASTM standards immediately following discharge from the mixer and prior to specimen casting. Slump (workability) was measured according to ASTM C143, with one measurement per mixture. Fresh concrete temperature was monitored using a calibrated digital thermometer in compliance with ASTM C1064. Air content was determined using the pressure method (ASTM C231, Type B meter). Unit weight was measured using a calibrated volumetric container (10 L capacity) in accordance with ASTM C138, with the unit weight calculated as the ratio of concrete mass to container volume.

2.4. Hardened Concrete Testing (Mechanical Properties)

2.4.1. Compressive Strength (ASTM C39)

Three cylindrical specimens (150 mm diameter × 300 mm height) per mixture per age (7, 14, and 28 days) were tested for axial compressive strength using a 2,000 kN capacity electrohydraulic testing machine (UTEST brand). Specimens were loaded at a constant rate of 0.25 ± 0.05 MPa/s (equivalent to 2.55 ± 0.51 kg/cm²/s) in accordance with NTP 339.034:2015 (equivalent to ASTM C39). No end-cap refacing was applied; instead, specimens were tested with their as-cast surfaces. Compressive strength was calculated as the ratio of maximum load to specimen cross-sectional area and reported in megapascals (MPa). The main features of the test setup for the compressive strength test are shown in Figure 5-a.

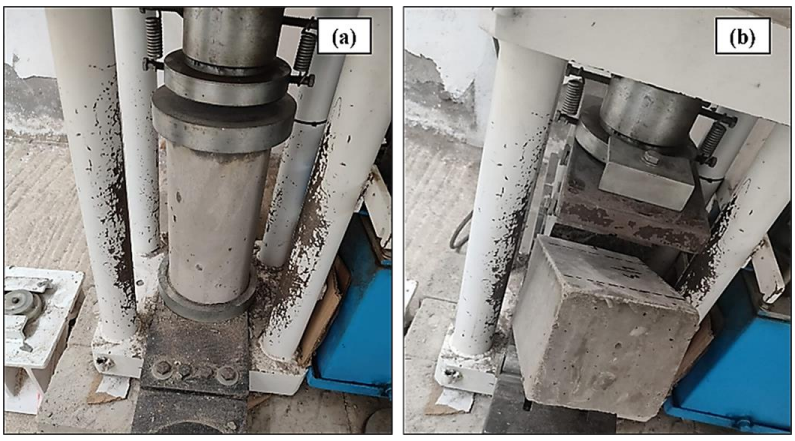

Figure 5. Compression and flexural strength tests

2.4.2. Flexural Strength (ASTM C78)

Three prismatic beam specimens (150 mm × 150 mm × 550 mm) per mixture per age (7, 14, and 28 days) were tested in third-point bending using the same 2,000 kN electrohydraulic testing machine. The clear span was 530 mm, and loading was applied at a constant rate of 0.86 to 1.21 MPa/min (equivalent to 8.77 to 12.34 kg/cm²/min) in compliance with NTP 339.034:2015. Modulus of rupture (MR) was calculated using the formula: $MR=3PL/2bh^2$, where P is the maximum applied load (N), L is the clear span (m), b is the beam width (m), and h is the beam depth (m). The main features of the flexural test setup are shown in Figure 5-b.

2.5. Durability Testing Program

2.5.1. Water Permeability

Water permeability was determined using a variable-head permeameter apparatus applied to cylindrical specimens (150 mm diameter × 300 mm height) at 56 days of age. The method follows principles outlined in ACI 522R-10, although applied to conventional (non-permeable) concrete. Specimens were installed in a test chamber with lateral sealing using O-rings to ensure unidirectional (axial) flow. Water at 20 ± 2°C was supplied from a graduated standpipe of 50 mm diameter. The coefficient of permeability k (cm/s) was calculated using the Darcy Equation 1:

$$k = (a \times L \times \ln(h_1 / h_2))/(A \times t) \quad (1)$$

where, a is the cross-sectional area of the standpipe (cm²), L is the specimen length (cm), h_1 and h_2 are the initial and final water column heights (cm), A is the specimen cross-sectional area (cm²), and t is the elapsed time (s). Three specimens per mixture (P1, P2, P3, P4) were tested, with k values reported as the mean ± standard deviation (SD) in cm/s.

2.5.2. Rapid Chloride Permeability (RCPT)

Chloride ion penetration resistance was assessed using the RCPT according to ASTM C1202. Cylindrical specimens (150 mm × 300 mm) at 28 and 56 days were cut into 50 mm thick disks using a diamond-blade saw. The disk was sealed laterally with an epoxy resin, leaving the top and bottom faces exposed. The specimen was placed in a test cell with a 3.0% sodium chloride solution on the cathode side and a 0.3 M sodium hydroxide solution on the anode side. A constant voltage of 60 V DC was applied across the specimen for 6 hours. Electrical current was recorded at 30-minute intervals. The total charge passed (Coulombs) was calculated by integrating the current-time curve. Three specimens per mixture (P1, P4) were tested at 28 and 56 days.

2.5.3. Sulfate Resistance (ASTM C1012)

Resistance to sodium sulfate attack was evaluated using mortar bars prepared from concretes according to ASTM C1012. Mortar samples (16 mm × 16 mm × 102 mm nominal) were extracted from the concrete mixtures. Bars were conditioned at 23 ± 2°C and > 95% RH for 56 days prior to exposure. Test bars were then immersed in a 5% sodium sulfate solution (Na_2SO_4, 50 g/L by mass) at 23 ± 2°C. Initial and final lengths were measured using a length comparator gauge with 0.1 mm resolution. Length change measurements were recorded at 7-day intervals over 56 days of exposure. Expansion (%) was calculated as $\Delta L/L_0 \times 100$, where ΔL is the change in length (mm) and L_0 is the initial length (150 mm). Three specimens per mixture (P1, P4) were tested, with results reported as percentage expansion at 56 days.

2.5.4. Accelerated Carbonation (UNE-EN 112011)

Accelerated carbonation testing was performed on cylindrical specimens (150 mm × 300 mm) at 28 and 56 days of curing in natural conditions. Specimens were preconditioned by drying at 23 ± 2°C and 50% RH until constant mass was achieved. Specimens were then exposed to a carbonation chamber with controlled conditions: CO_2 concentration of 20–25% (v/v), relative humidity of 60–70%, and temperature of 20–25°C in compliance with UNE-EN 112011. Following exposure, specimens were split along their length, and the carbonation depth was measured on the freshly exposed surface using 1% phenolphthalein solution in ethanol. The color change boundary (pink to colorless) was marked and measured at 5 locations per specimen using a digital caliper with 0.1 mm resolution. Three specimens per mixture (P1, P2, P3, P4) were tested at 28 and 56 days, with results reported as mean carbonation depth ± standard deviation in millimeters.

2.5.5. Ultrasonic Pulse Velocity-UPV (ASTM C597)

UPV measurements were performed on intact cylindrical specimens (150 mm diameter × 300 mm height) at 28 and 56 days using a Proceq Pundit ultrasonic testing device. The equipment was equipped with longitudinal transducers operating at 500 kHz and was calibrated using the manufacturer-supplied reference rod (25.4 µs) prior to all

measurements. Specimens were placed in direct transmission mode with transducers positioned at opposite ends of the cylinder. Ultrasonic coupling gel was applied to ensure acoustic contact. For each specimen, three consecutive readings were recorded, and the average transit time was calculated. Velocity was computed as V = L/t, where L is the distance between transducers (m) and t is the average transit time (s). Three specimens per mixture (P1, P4) were measured at 28 and 56 days, with results reported in m/s as mean ± standard deviation.

2.5.6. Surface Abrasion Resistance (ASTM C944)

Abrasion resistance was evaluated by the rotating-cutter method according to ASTM C944. A benchtop electric column drill was adapted as the abrasion apparatus per standard specifications. Cylindrical specimens (150 mm × 300 mm) at 28 and 56 days were secured in a mechanical vise, and a hardened steel cutter (diameter 3 mm) was applied with a normal load of 98 N at a rotational speed of 200 ± 10 rpm. The depth of abrasion (penetration) was recorded at regular intervals. The cutter was continuously applied for the specified duration, after which the specimen was removed, cleaned, and weighed to the nearest 0.1 g. Mass loss (in grams) was used as the measure of abrasion resistance. Three specimens per mixture (P1, P4) were tested at 28 and 56 days, with results reported as mean mass loss ± standard deviation in grams.

2.6. Microstructural Analysis (XRD, FTIR, SEM)

2.6.1. Sample Preparation

Samples for microstructural analysis were obtained from cylindrical specimens at 28 days of age. Cores were extracted from the central region of each specimen using a diamond-core drill, then sectioned using a diamond-blade wet saw. Fragments approximately 5–10 mm in size were prepared and ground to particle sizes < 75 μm using an agate mortar. Samples were not subjected to active hydration-stopping procedures (e.g., solvent immersion or freeze-drying) but were analyzed as received to reflect the in-situ condition. All samples were stored in sealed containers at room temperature until analysis.

2.6.2. X-ray Diffraction (XRD)

Phase composition was determined by powder X-ray diffraction (XRD) using a Rigaku Ultima IV diffractometer equipped with Cu-Kα radiation (λ = 1.5406 Å) operating at 40 kV and 40 mA. Samples were scanned in the 2θ range of 5° to 70° at a rate of 0.04° per second. Phase identification was performed using the PDXL software suite (Rigaku) with reference to the International Centre for Diffraction Data (ICDD) PDF-4 database. Semi-quantitative phase analysis was conducted using the Rietveld refinement method to determine relative abundances of major crystalline phases including C_3S, C_2S, C_3A, C_4AF, portlandite ($Ca(OH)_2$), and C-S-H gel. Results are presented for control concrete (P1) and the optimal experimental mixture (P4) at 28 days.

2.6.3. Fourier-Transform Infrared Spectroscopy (FTIR)

Infrared absorption spectra were recorded using a Perkin Elmer Frontier FTIR spectrometer equipped with a diamond attenuated total reflection (ATR) accessory. Samples (powdered, < 75 μm) were placed directly on the ATR crystal and analyzed in the wavenumber range of 400 to 4,000 cm^{-1} with a spectral resolution of 4 cm^{-1} and 32 accumulated scans per sample. Characteristic absorption bands were identified and assigned to functional groups including Si–O stretches (silicates), C–H stretches (aliphatic), O–H stretches (hydroxides and water), and C=O stretches (carbonates). Spectral interpretation was performed by comparison with reference spectra of pure cement phases, Aloe vera gel, and Sika®-1 admixture. Results are compared between control (P1) and optimal mixture (P4) to identify chemical transformations resulting from the combined additives.

2.6.4. Scanning Electron Microscopy (SEM)

Microstructural morphology and interfacial characteristics were examined using a FEI Quanta 650 scanning electron microscope (FEI, Hillsboro, OR, USA). Specimens were fracture-exposed from 28-day-old cylindrical samples, mounted on aluminum stubs, and coated with a thin layer of gold (Au) using a sputter coater to enhance surface conductivity. Imaging was performed under high vacuum conditions at an accelerating voltage of 20 kV. Secondary electron (SE) images were acquired at multiple magnifications (500×, 1,000×, 5,000×, and 10,000×) to assess cement hydrate morphology, pore structure, C-S-H gel formation, and the interfacial transition zone (ITZ) microstructure.

2.7. Large-Scale Structural Validation (Pilot Test)

2.7.1. Selection of Optimal Mixture

The optimal mixture was selected based on multi-criteria assessment incorporating (i) compressive strength at 28 days, (ii) flexural strength at 28 days, and (iii) durability indicators (water permeability and ultrasonic pulse velocity at

56 days). The experimental mixture demonstrating the best balance of enhanced mechanical performance and superior durability compared to the control (P1) was designated as the "optimal" mixture and was selected for structural-scale validation testing.

2.7.2. Inverted U-Frame (Vertical Loading)

A reinforced concrete frame scaled at 1:4 was constructed and tested under monotonic vertical loading. The frame consisted of two vertical columns (50 mm × 50 mm cross-section, 600 mm height) and a horizontal beam (50 mm width × 70 mm depth, 700 mm clear span) connected in an inverted U configuration. All critical connections were designed as fixed (fully moment-resisting). Longitudinal reinforcement comprised 6 mm diameter deformed steel bars (grade 60) placed continuously along the beam with 180° hooks at the ends. Transverse reinforcement (stirrups) was not provided to allow for brittle failure modes characteristic of non-ductile design.

The frame was secured at both column bases to a rigid test bed using mechanical anchors (fixed boundary conditions). A concentrated vertical load was applied at the midpoint of the beam span using a loading ram connected to a 1,000 kN capacity electrohydraulic testing machine. Load was applied incrementally at a constant rate of 0.86 to 1.21 MPa/min (equivalent to 8.77 to 12.34 kg/cm²/min) until failure or attainment of maximum machine capacity. Deflection was monitored using linear variable displacement transducers (LVDTs) positioned vertically beneath the load point and at key locations along the frame. Strain gauges were bonded to longitudinal reinforcement at critical sections to record tension development.

2.7.3. C-Shaped Frame (Horizontal Joint Loading)

A second scaled frame (1:4) was constructed in a C-shaped configuration to simulate lateral (in-plane shear) loading on the beam-column joint. The C-frame consisted of a single vertical column (50 mm × 50 mm cross-section) and a horizontal cantilever beam (50 mm × 70 mm section, 400 mm length) connected at the top via a fixed joint (Figure 6). The base of the column was anchored to a rigid foundation (fixed boundary condition).

Horizontal load was applied at the column-beam junction using a mechanical loading device attached to the testing machine at a height coinciding with the joint centerline. Load was incremented monotonically at 0.86 to 1.21 MPa/min until failure. Lateral displacement (drift) of the beam end was measured using LVDTs. Strain gauges were installed at the column base and joint region to record shear stress distribution. Both frame tests were conducted using concrete from the control (P1) and optimal (P4) mixtures to enable direct comparison of structural performance. All frames were cast from the same concrete batches, cured under identical conditions, and tested at 28 days of age.

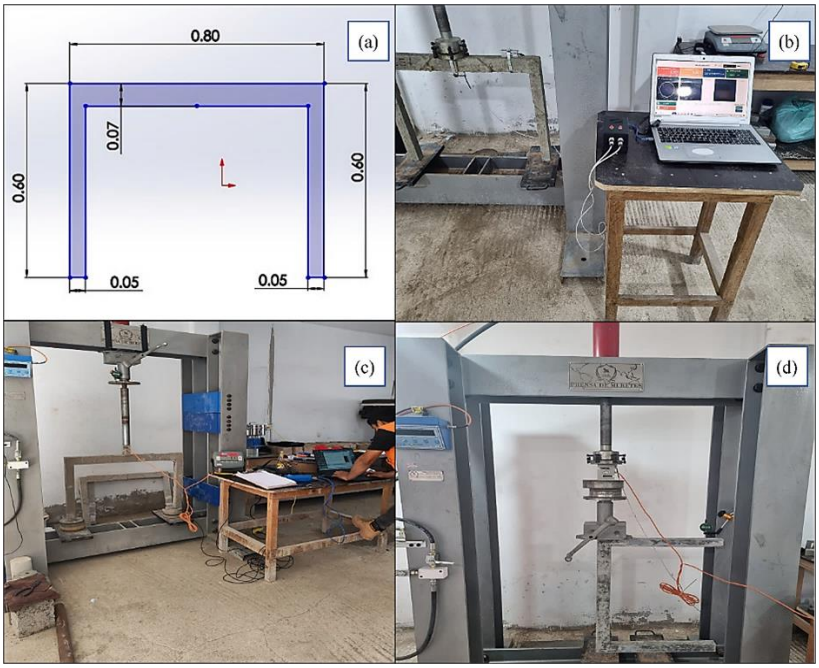

Figure 6. Procedure for structural validation in scale frames

2.8. Cost–Benefit Analysis Methodology

An economic performance index was calculated based on the methodology adapted from Yu et al. [35], which integrates material costs with normalized indices of mechanical and durability performance. The cost–benefit index G_i was defined as (Equation 2):

$$G_i = \frac{C_0 \cdot P_i}{C_i \cdot P_{P1}} \quad (2)$$

where, C_0 and C_i are the unit costs ($/m³) of control and experimental mixtures, respectively, and P_i and $P_1$are the normalized performance indices (dimensionless) for experimental and control mixtures.

The performance index P_i was constructed as a weighted sum of mechanical and durability indicators:

$$P_i = w_m \cdot I_m + w_d \cdot I_d \quad (3)$$

where, w_m and w_d are weighting factors for mechanical and durability indices (set to 0.5 each for equal importance), I_m is the normalized mechanical index, and I_d is the normalized durability index.

The mechanical index I_m was calculated as the average of normalized compressive strength and flexural strength at 28 days:

$$I_m = \frac{1}{2}\left(\frac{f'_{c,i}}{f'_{c,P1}} + \frac{MR_i}{MR_{P1}}\right) \quad (4)$$

The durability index I_d incorporated normalized indicators of water permeability and ultrasonic pulse velocity at 56 days, with inversions applied for permeability (lower is better):

$$I_d = \frac{1}{2}\left(\frac{k_{P1}}{k_i} + \frac{UPV_i}{UPV_{P1}}\right) \quad (5)$$

All strength and transport properties were normalized relative to control mixture P1 (P_1 = 1.0). Material costs were obtained from local suppliers in Chiclayo, Lambayeque, and are itemized as follows: Portland cement Type I = $0.33/kg ($14.00/42.5 kg bag); fine aggregate = $22/m³; coarse aggregate = $26/m³; Sika®-1 = $1.50/kg; *Aloe vera* gel = $0.40/kg; water = $0/m³. The cost index for control concrete (C_0) was calculated by summing the unit costs of all constituents at design quantities, and similar calculations were performed for each experimental mixture (Ci).

3. Results and Discussion

3.1. Chemical Characterization of Additives (Sika®-1 and Aloe vera)

The chemical characterization of additives is fundamental to understanding their synergistic interaction mechanisms within the cement matrix. Sika®-1, a commercial colloidal silicate-based integral waterproofing admixture, and Aloe vera gel, a bio-based polysaccharide-rich material, were selected for their complementary physico-chemical properties. The former provides capillary pore blockage through colloidal silicate precipitation and $CaCl_2$ -accelerated densification, while the latter contributes viscosity modulation and potential water-retention capacity via its polysaccharide network (primarily acemannan). Table 3 presents the key physico-chemical parameters that govern their behavior in fresh and hardened concrete.

Table 3. Physico-chemical properties of chemical and bio-based additives

Property	Test Method/Equipment	Sika®-1 (S1)	*Aloe vera* Gel (AV)	Functional Implication
pH (20°C)	Potentiometric titration (ASTM E70)	8.5 ± 0.1	7.2 ± 0.2	Pore solution compatibility
Density (g/cm³)	Pycnometry (ASTM D854)	1.00 ± 0.02	1.030 ± 0.005	Homogeneous dispersion
Solid's content (% w/w)	Gravimetry (105°C, 24 h)	18.5 ± 2.5	0.10 ± 0.01	Colloidal vs. dissolved mechanism
Dynamic viscosity (cP, 25°C)	Brookfield viscometer (ASTM D2196)	N/R	450 ± 35	Rheology modification potential
Active ingredient	—	Colloidal sodium silicate / $CaCl_2$	Acemannan (polysaccharide)	Electrosteric vs. steric stabilization

The alkaline nature of S1 (pH 8.5) aligns with typical silicate-based waterproofing admixtures, ensuring compatibility with the cement pore solution (pH 12-13) without premature hydrolysis of ester linkages. In contrast, Aloe vera gel exhibited near-neutral pH, minimizing potential acidic interference with calcium silicate hydration. The density differential ρ_{S1} vs. ρ_{AV}, remained within negligible range (<3%), ensuring homogeneous distribution during mixing. Notably, the ultra-low solids content of AV (0.1% w/v) indicates that its functional contribution derives primarily from dissolved polysaccharides rather than particulate matter, contrasting with the 15-25% solids fraction of Sika®-1 that provides colloidal stabilization.

3.2. Fresh Concrete Properties

The fresh properties of the four mixtures are presented in Figure 7. The slump values recorded across all mixtures (4.0–4.5 inches) remained within acceptable limits for conventional concrete placement (ASTM C143: 2.0–6.0 inches),

demonstrating that the integrated admixture system did not impair workability during the critical mixing and casting window. P2 (4%S1+1%AV) exhibited the maximum slump of 4.5 inches, representing a 12.5% increase relative to the control, which is consistent with established understanding of polycarboxylate-based superplasticizers' electrosteric dispersion effect. Conversely, P4 (3%S1+2%AV) returned to the control slump value of 4.0 inches despite containing admixtures, suggesting a rheological compensation mechanism. This observation aligns with the findings of Pang et al. [32], who demonstrated that polysaccharide additives at concentrations exceeding 1.5% by cement weight induce viscosity-mediated flow restriction through intermolecular hydrogen bonding, thereby offsetting the flow-enhancing properties of polycarboxylates.

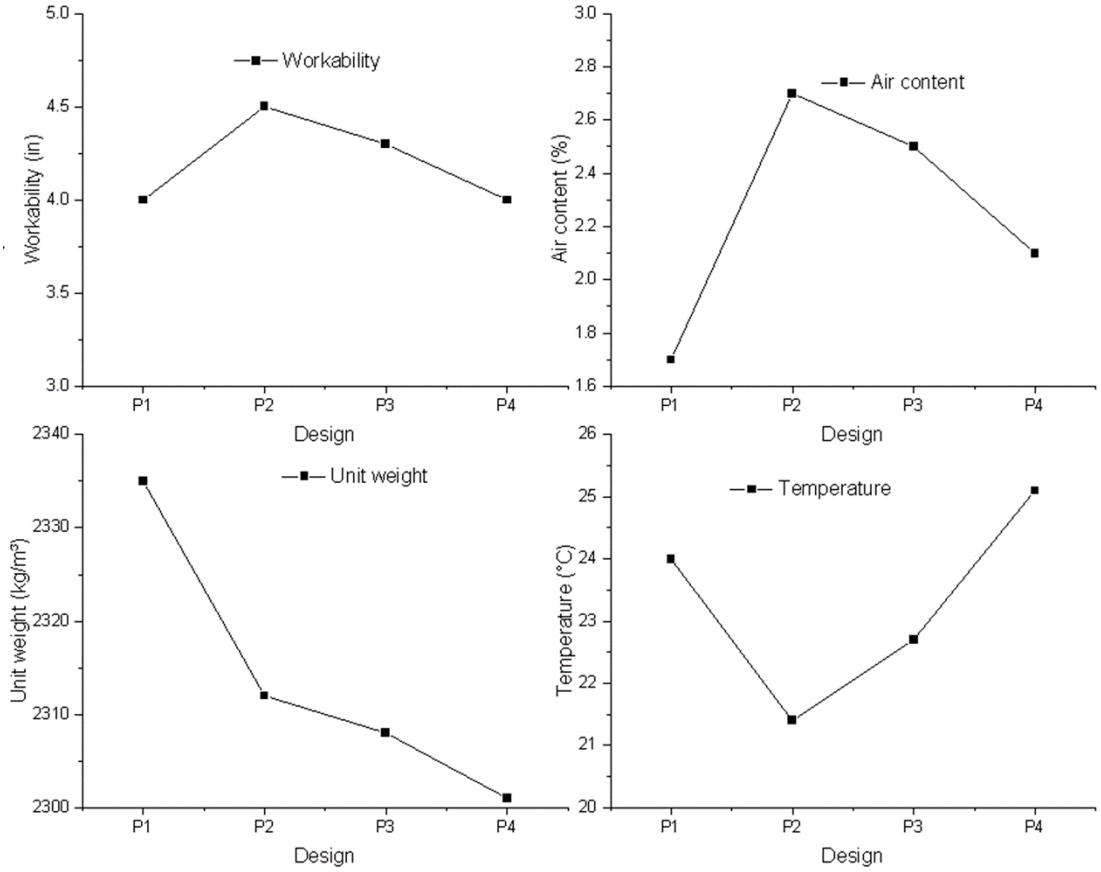

Figure 7. Properties of fresh concrete by mix design

Ambient temperature during mixing remained stable across all batches (21.4–25.1 °C), well within the ASTM C1064 recommended range of 16–32 °C. The 3.7 °C temperature differential between P2 and P4 reflects uncontrolled ambient variation rather than exothermic effects from admixture interaction, as documented by Yehia et al. [39], who confirmed that polycarboxylate additions at dosages below 5% contribute negligibly to concrete temperature rise.

Air content increased progressively in admixture-containing mixtures (2.1–2.7%) relative to the control (1.7%), representing a 24–59% relative increase. This phenomenon is characteristic of polycarboxylate-based systems and has been thoroughly documented by Palacios et al. [28], who attributed air entrainment to enhanced bubble stabilization via electrostatic surface charge. Unit weight declined systematically with increasing admixture incorporation, from 2335.3 kg/m³ (P1) to 2301.1 kg/m³ (P4), a 1.47% reduction consistent with increased air void content. Mass-balance calculations indicate that admixture contribution accounts for 53% of the unit weight loss (18.15 kg/m³), while increased air voids account for the remaining 47% (16.05 kg/m³), a partitioning confirmed by ASTM C138 gravimetric relationships.

3.3. Mechanical Strength Development (Compression and Flexure)

Compressive strength development for the four mixtures is shown in Figure 8-a, while flexural strength at corresponding ages is given in Figure 8-b. Compressive strength development followed the typical sigmoid curve of Portland cement hydration, with accelerated gains between 7 and 28 days. At 7 days, P4 achieved 20.67 ± 0.32 MPa, representing a 12.4% improvement over the control, suggestive of accelerated early-age hydration kinetics. This

early-age enhancement is consistent with research by Chen et al. [3], who reported 10–15% strength gains at 7 days when combining waterproofing admixtures with bio-based polysaccharides. The mechanism underlying this acceleration likely involves: (i) reduced nucleation barrier for C-S-H gel formation due to calcium-polysaccharide complexation, and (ii) enhanced ionic transport via viscosity reduction in the pore solution by dissolved biopolymers. By 28 days, P4 attained 28.77 ± 0.10 MPa, representing an 8.9% improvement over the control's 26.40 ± 0.65 MPa. This more modest gain at 28 days compared to 7 days reflects the convergence of hydration rates at later ages, where the control mixture's cement hydration fully matures. P2 similarly exceeded the control at 28.37 ± 0.41 MPa (7.5% improvement), whereas P3 fell slightly below at 25.73 ± 0.06 MPa, suggesting an optimal balance of additive dosages at P2 and P4 compositions.

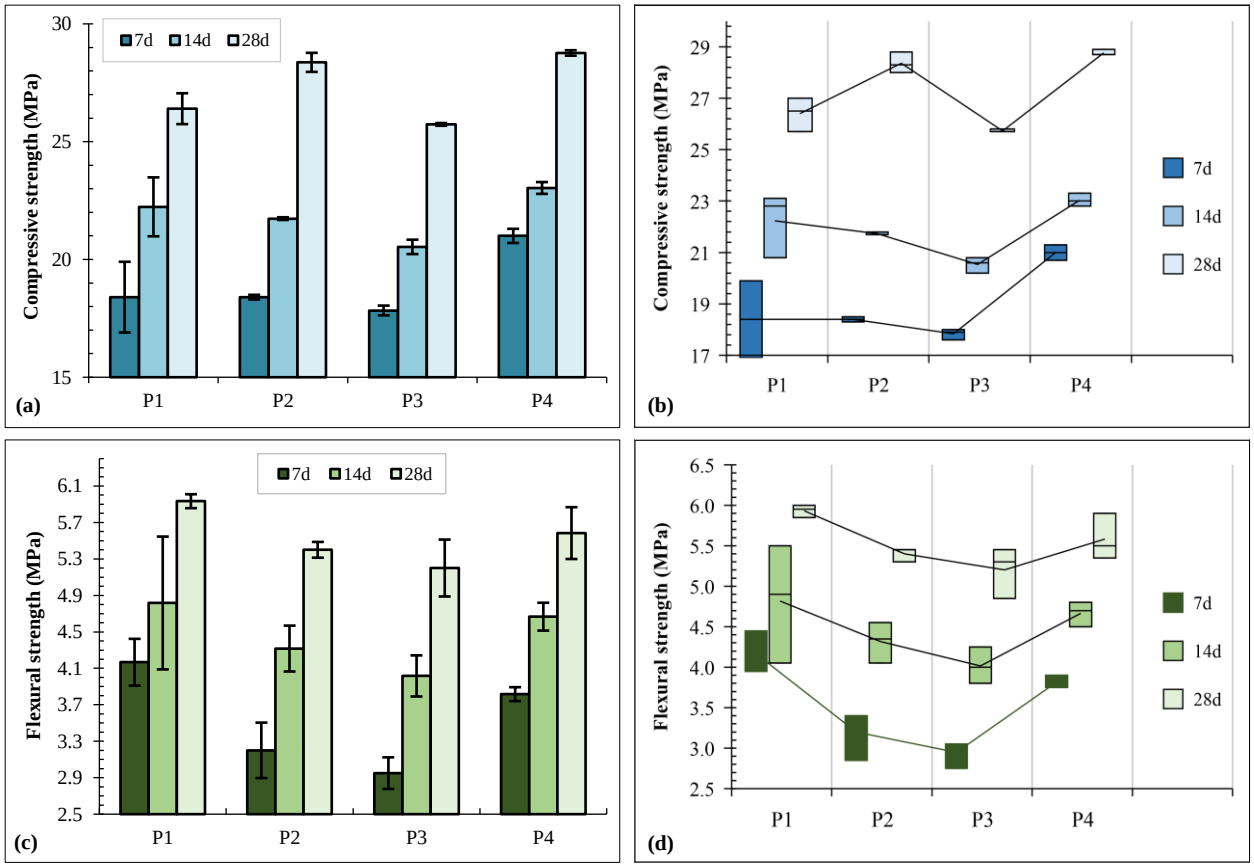

Figure 8. Mechanical properties of hardened concrete by mix design

Modulus of rupture (flexural strength) measurements at 28 days revealed that the control mixture (P1) maintained the highest MR of 5.93 ± 0.08 MPa, while P4 achieved 5.58 ± 0.28 MPa, equivalent to 94.1% of the control (Figure 8-c). This represents a 6% reduction in flexural performance relative to compressive strength gains, indicating that while admixtures enhance matrix densification and compressive capacity, they may slightly compromise flexural toughness and crack propagation resistance. This trade-off is consistent with observations by Zhang et al. [40], who documented that polysaccharide-based admixtures improve stiffness-related properties but can marginally reduce the plastic deformation capacity of the concrete microstructure. The comparative trend across all mixtures (P1 > P2 > P4 > P3) suggests that excessive polysaccharide content (P3: 1.5%AV) may induce excessive pore refinement, creating a brittle microstructure prone to sudden failure. P4, with a higher biopolymer dosage (2.0%AV) but lower waterproofing admixture (3.0%S1), appears to balance these competing mechanisms more effectively than P3, although compressive and flexural strength optima occur at slightly different dosage combinations.

The 8.9% increase in compressive strength in P4 is within the range reported for individual bio-additive systems (6.1–10.2%), as per Table 4, confirming that the hybrid formulation achieves improvements in durability (Figures 9 and 10) without compromising mechanical performance. The substantially greater increase reported by Barco-Tocto et al. [12] for combinations of nopal and aloe vera obtained a different and higher resistance result for a higher total dose of additive, which prevents a direct comparison, but indicates the significant contribution of the additive on the strength of the concrete. The distinguishing feature of the present study is that none of the references cited integrated microstructural characterization (XRD, FTIR, SEM), pilot-scale structural validation and techno-economic analysis within a single experimental program.

Table 4. Comparison of compressive strength with previous studies on bio-admixture concrete

Study	Admixture system	Dosage (% bwoc)	f'c (MPa)	Δ vs. control (%)
Present study — P4	Sika-1 + Aloe vera	3.0%S1 + 2.0%AV	28.77	+8.9
Oshim et al. [24]	Aloe vera gel alone	2.0% AVG	31.42	+10.2
Suwondo et al. [15]	Crystalline WA alone	2.0% CWA	43.50	+6.1
Barco-Tocto et al. [12]	Nopal + Aloe vera	2%N + 0.5%AV	43.47	+80.7*
Ahmed et al. [10]	Aloe vera gel alone	2.5% AVG	~23.0	+57% workability
Abdellatief et al. [41]	Sika Viscocrete	Variable	23.10	+31.0

* Design strength 245 kg/cm²; not directly comparable to the present f'c 21 MPa design.

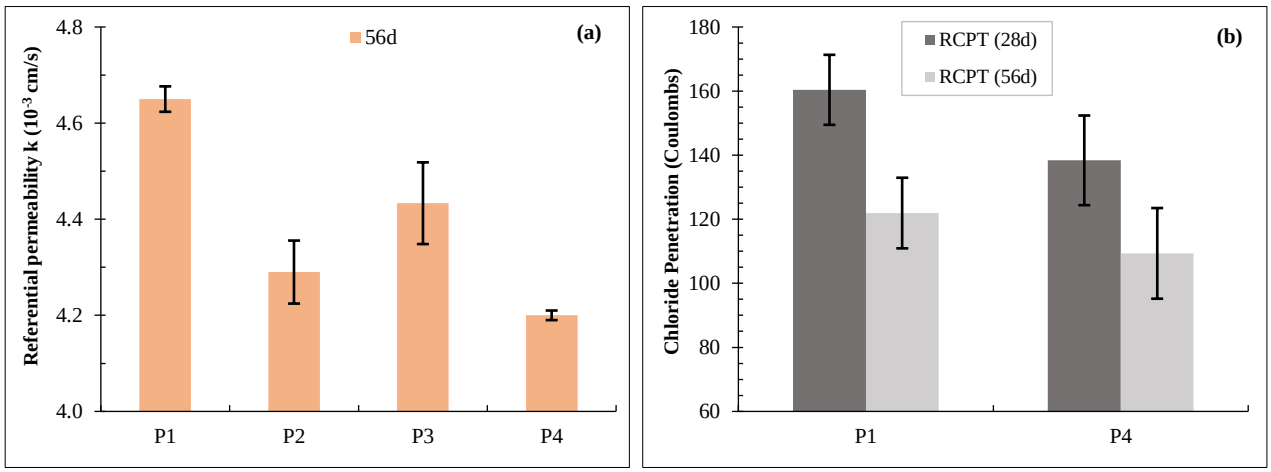

Figure 9. Transport durability properties

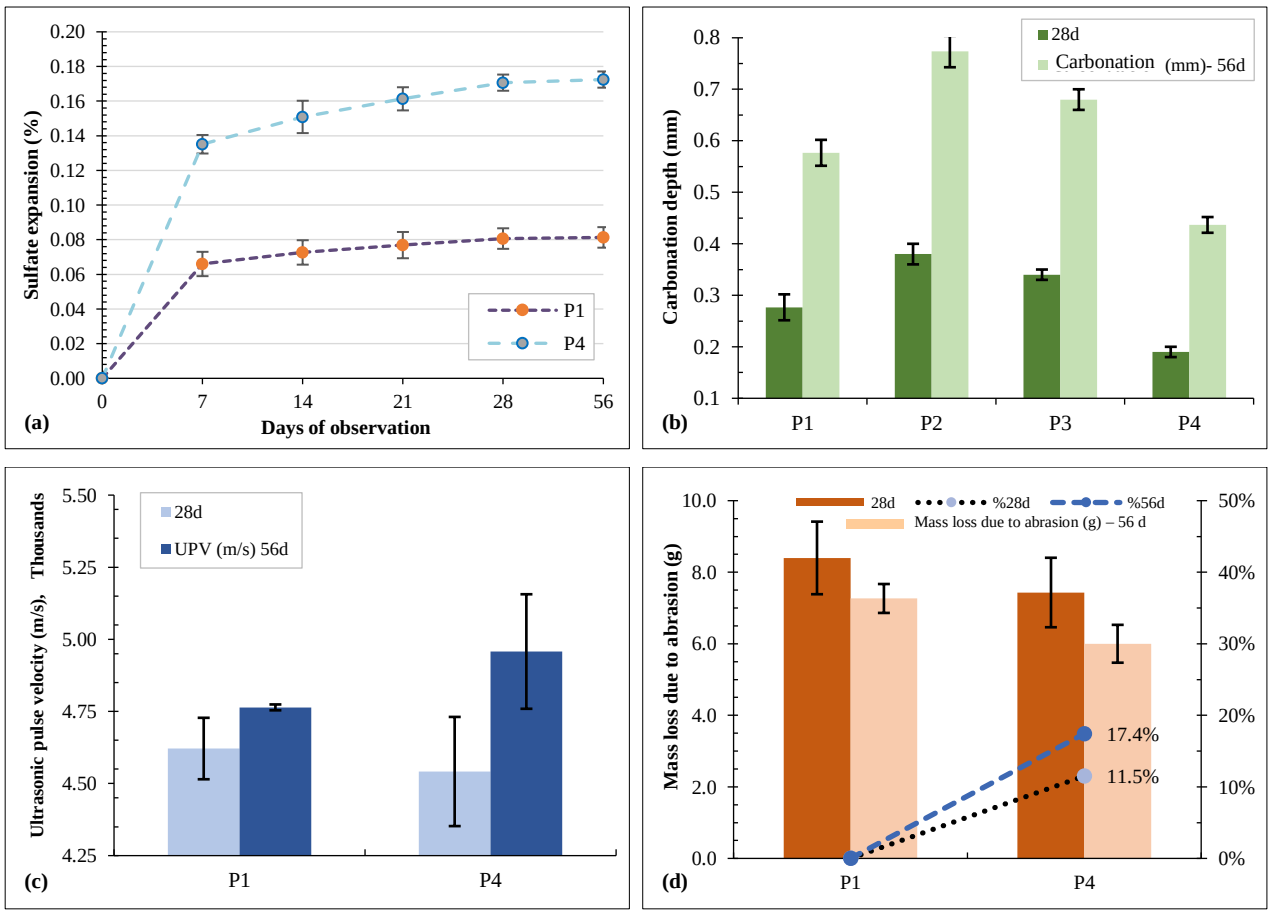

Figure 10. Durability properties regarding resistance to chemical attack, UPV and abrasion

Inferential analysis confirmed that mixture composition exerted a statistically significant effect on both 28-day mechanical responses (Table 5), although the magnitude of this effect was clearly stronger for compressive behavior than for flexural behavior. The post hoc pattern indicates that the hybrid formulations produced a sharper discriminatory response in compression, whereas flexural performance remained comparatively less sensitive to dosage variation and showed only limited pairwise separation among mixtures. Taken together, these results suggest that the Sika-1/Aloe vera system primarily modified matrix densification and load-bearing capacity under compression, while its influence on bending-related behavior was more moderate.

Table 5. One-way ANOVA summary for 28-day compressive and flexural strength of mixtures P1–P4

Response variable	P1	P2	P3	P4	ANOVA FFF	p-value	η^2	Significant Tukey HSD contrasts
Compressive strength (MPa)	26.40 ± 0.66	28.37 ± 0.40	25.73 ± 0.06	28.77 ± 0.12	42.97	0.000	0.94	P1 vs. P2; P1 vs. P4; P2 vs. P3; P3 vs. P4
Flexural strength (MPa)	5.93 ± 0.08	5.40 ± 0.09	5.20 ± 0.31	5.58 ± 0.28	6.08	0.018	0.7	P1 vs P3

3.4. Durability Performance

3.4.1. Transport Properties (Permeability, Chloride Penetration)

The permeability and RCPT results are plotted in Figure 9. Water permeability testing at 56 days demonstrated marked improvements in transport resistance for all admixture-containing mixtures. P4 exhibited the lowest permeability coefficient of 0.00420 ± 0.00001 cm/s, representing a 9.7% reduction relative to the control's 0.00465 ± 0.00003 cm/s. The extremely low standard deviation in P4 (±0.00001 cm/s) across three replicate specimens indicates exceptional consistency and reproducibility, suggesting that the additive combination produces a stable, uniform pore structure resistant to experimental variability. This finding contrasts with the control mixture's higher variability (±0.00003 cm/s), implying that admixture-stabilized microstructures exhibit more uniform permeability characteristics. The permeability reduction mechanism combines two complementary effects: (i) crystalline mineral precipitation from the silicate-based waterproofing agent, which physically blocks capillary pathways, and (ii) refined pore structure from biopolymer-promoted C-S-H gel densification, which reduces pore size distribution and connectivity. These improvements have direct implications for service life extension, as water ingress is the primary vector for deleterious ion transport and corrosion initiation in reinforced concrete structures.

Rapid chloride permeability testing at 28 and 56 days confirmed strong resistance to chloride ion penetration in both control and optimal mixtures. P4 demonstrated 13.7% lower charge passage at 28 days (138.38 ± 14.00 C vs. 160.39 ± 10.93 C) and 10.3% lower at 56 days (109.34 ± 14.15 C vs. 121.93 ± 11.02 C), both classified as having 'Very Low' chloride permeability per ASTM C1202 (100–1,000 Coulombs). The reduction in charge passage over time (both mixtures exhibiting ~10% reduction from 28 to 56 days) reflects continued hydration and microstructural densification. The mechanism of chloride resistance improvement in P4 likely involves reduced pore connectivity and increased chloride binding capacity at the C-S-H surface due to enhanced gel formation and reduced calcium hydroxide content (a less durable phase). These findings have substantial practical implications for marine infrastructure and coastal structures, where chloride ingress from salt spray or seawater exposure accelerates reinforcement corrosion; a 13.7% reduction in ionic transport translates to extended time-to-corrosion initiation, potentially adding years to the structure's useful life.

The 13.7% reduction in chloride permeability at 28 days recorded for P4 is consistent in direction, though more moderate in magnitude, than the 53–65% water penetration reductions reported by Suwondo et al. [15] for CWA alone at 1–2% dosage. The comparatively modest improvement observed here reflects the lower Sika-1 content in P4 (3.0% bwoc) and the partial substitution of inorganic waterproofing agent by biopolymer gel. A dual-mechanism framework explains the synergistic transport improvement: the silicate-based admixture seals residual microcapillaries (diameter >10 μm) through crystalline precipitation, while the Aloe vera polysaccharide network refines mesopores (1–10 μm) by promoting additional C-S-H nucleation at the gel–pore interface. Neither admixture, applied alone at its respective dosage, would be expected to modify both pore size ranges simultaneously [11].

3.4.2. Resistance to Chemical Attack and Abrasion

Contrary to expectations, P4 exhibited higher expansive strain upon 56-day exposure to 5% sodium sulfate solution compared to the control: 0.0911% (P4) versus 0.0813% (P1), representing a 12.05% relative increase in expansion. This unexpected result suggests that the admixture combination, despite improving resistance to water and chloride ingress, may reduce overall sulfate resistance through phase composition modifications. The likely mechanism involves suppression of ettringite formation (a characteristic sulfate expansion product) due to reduced available aluminum from the C-S-H gel or precipitation of hydration products that consume precursor sulfate before expansion-promoting phases

can form. This finding highlights an important durability trade-off: the optimal mixture P4 excels in chloride and carbonation resistance (environments typical of tropical coastal and urban infrastructure) but shows reduced sulfate tolerance (relevant to arid, industrial, or subsurface exposures). Practical application of this mixture should therefore prioritize environments with limited sulfate exposure risk and high chloride or carbonation threat. Wang et al. reviewed the competitive interaction between crystalline waterproofing materials and sulfate attack, demonstrating that both processes consume available Ca^{2+} from the cement pore solution, the waterproofing agent to precipitate pore-blocking silicate crystals, and sulfate ions to form expansive ettringite ($3CaO{\cdot}Al_2O_3{\cdot}3CaSO_4{\cdot}32H_2O$) and gypsum. In P4, the combined Ca^{2+} demand from silicate crystallization, biopolymer complexation, and sulfate reaction may have reduced the calcium reservoir available for buffering ettringite growth, thereby allowing marginally greater sulfate-driven expansion. Ettringite crystallization within pores of 10–50 nm diameter has been shown to generate internal stresses exceeding 8 MPa, sufficient to initiate microcracking in otherwise dense matrices. This mechanistic interpretation reconciles the apparently contradictory observation of improved chloride and carbonation resistance alongside reduced sulfate tolerance, and reinforces the recommendation that P4 be deployed preferentially in chloride- or carbonation-dominated exposure classes (XS, XC per EN 206) rather than sulfate-rich environments (XA) [19, 42, 43].

Accelerated carbonation testing at 56 days revealed that P4 achieved the lowest carbonation depth of 0.44 ± 0.02 mm, compared to the control's 0.58 ± 0.03 mm, representing a 24.1% reduction. P2 showed substantially higher carbonation (0.77 ± 0.03 mm), indicating that excessive waterproofing admixture dosage (4.0%S1) may paradoxically compromise carbonation resistance, possibly through reduced portlandite (CH) content available for buffering CO_2. The inverse relationship between waterproofing admixture dosage and carbonation resistance suggests that the silicate-based waterproofing mechanism, while effective for capillary blockage, does not necessarily protect against gaseous CO_2 diffusion. The 24.1% reduction in carbonation depth in P4 carries significant durability implications, as carbonation penetration is a primary driver of reinforcement corrosion in non-chloride-contaminated environments. The carbonation rate relationship implies that a 24% reduction in carbonation depth at 56 days translates to approximately 44% extended time-to-neutralization of the concrete cover zone, substantially prolonging corrosion protection.

UPV measurements at 28 and 56 days revealed that both P1 and P4 exhibited "Excellent" quality per ASTM C597 classification. P1 measured 4621 ± 107 m/s at 28 days and 4764 ± 10 m/s at 56 days, while P4 measured 4542 ± 189 m/s at 28 days and 4924 ± 815 m/s at 56 days. The notably higher velocity in P4 at 56 days (4924 m/s, 3.4% above P1) suggests continued densification and reduced microcracking in the admixture-containing mixture, consistent with improved hydration product formation. The elevated standard deviation in P4 at 56 days (815 m/s) likely reflects localized variation in admixture distribution rather than systematic degradation, as the mean velocity remains in the "Excellent" range. The combined trends for sulfate expansion, carbonation depth, UPV, and abrasion mass loss are summarized in Figure 10.

3.4.3. Statistical Analysis of Results at 56 Days

Among the six durability indicators evaluated at 56 days (Table 6), mixture composition exerted a statistically significant effect on water permeability ($p < 0.001$), carbonation depth ($p < 0.001$), and abrasion mass loss ($p = 0.030 < 0.05$), while differences in rapid chloride permeability, sulfate expansion, and ultrasonic pulse velocity did not attain statistical significance at the $\alpha = 0.05$ threshold. Carbonation depth yielded the largest effect size across the entire dataset ($\eta^2 = 0.977$), with Tukey post hoc contrasts confirming statistically distinct separation among all four mixtures, a result that reflects the opposing behavior of the biopolymer-dominant formulation (P4, lowest depth) and the Sika-1-dominant formulation (P2, highest depth), suggesting that increased Aloe vera dosage promotes denser C–S–H that impedes CO_2 diffusion more effectively, while excess waterproofing admixture at this dosage level does not confer equivalent carbonation resistance. The non-significant outcomes for RCPT, sulfate expansion, and UPV should be interpreted with caution given the reduced statistical power inherent in two-group designs.

Table 6. One-way ANOVA summary for 56-day durability properties across available mixture groups

Durability property	P1 ($\bar{x}$ ± SD)	P2 ($\bar{x}$ ± SD)	P3 ($\bar{x}$ ± SD)	P4 ($\bar{x}$ ± SD)	*F*	*p*-value	η^2	Significant Tukey HSD contrasts
Water permeability, *k* (cm/s)	$4.65\times10^{-3} \pm 2.65\times10^{-5}$	$4.29\times10^{-3} \pm 6.56\times10^{-5}$	$4.43\times10^{-3} \pm 8.51\times10^{-5}$	$4.20\times10^{-3} \pm 1.00\times10^{-5}$	37.47	< 0.001	0.93	P1 vs. P2; P1 vs. P3; P1 vs. P4; P3 vs. P4
Carbonation depth (mm)	0.577 ± 0.025	0.773 ± 0.031	0.680 ± 0.020	0.437 ± 0.015	113.74	< 0.001	0.98	All pairs significant
Rapid chloride permeability (C)	121.93 ± 11.02	–	–	109.34 ± 14.15	1.479	0.291	0.27	NS
Sulfate expansion (%)	0.0813 ± 0.0059	–	–	0.0911 ± 0.0047	5.029	0.088	0.56	NS
Ultrasonic pulse velocity (m/s)	4764 ± 10	–	–	4958 ± 199	2.847	0.167	0.42	NS
Abrasion mass loss (g)	7.27 ± 0.40	–	–	6.00 ± 0.53	10.857	0.03	0.73	Significant pair.

3.5. Microstructural Analysis (Control vs. Optimal Mixture)

3.5.1. X-ray Diffraction (XRD)

Representative XRD patterns for the control and P4 mixtures are presented in Figure 11. Phase composition analysis via XRD at 28 days identified characteristic Portland cement hydration products in both P1 and P4 mixtures. P4 exhibited increased calcite ($CaCO_3$) content at 18.2% compared to P1's 14.6%, consistent with accelerated carbonation fronts penetrating the surface during the first 28 days of exposure. Albite (feldspar) phase content decreased from 40.0% (P1) to 28.9% (P4), suggesting partial reaction or surface dissolution of feldspathic aggregate during hydration, possibly influenced by the altered pore solution pH and ionic composition induced by the biopolymer additive. A critical limitation of XRD analysis for concrete specimens is that hydration products, particularly the C-S-H gel, which accounts for ~60% of mature cement paste, exhibit predominantly amorphous structure and thus escape quantification by conventional diffraction methods. The XRD results therefore reflect primarily aggregate mineralogy rather than cement hydration phase distribution. Complementary FTIR analysis (Section 3.5.2) provides superior sensitivity to amorphous C-S-H and functional group chemistry.

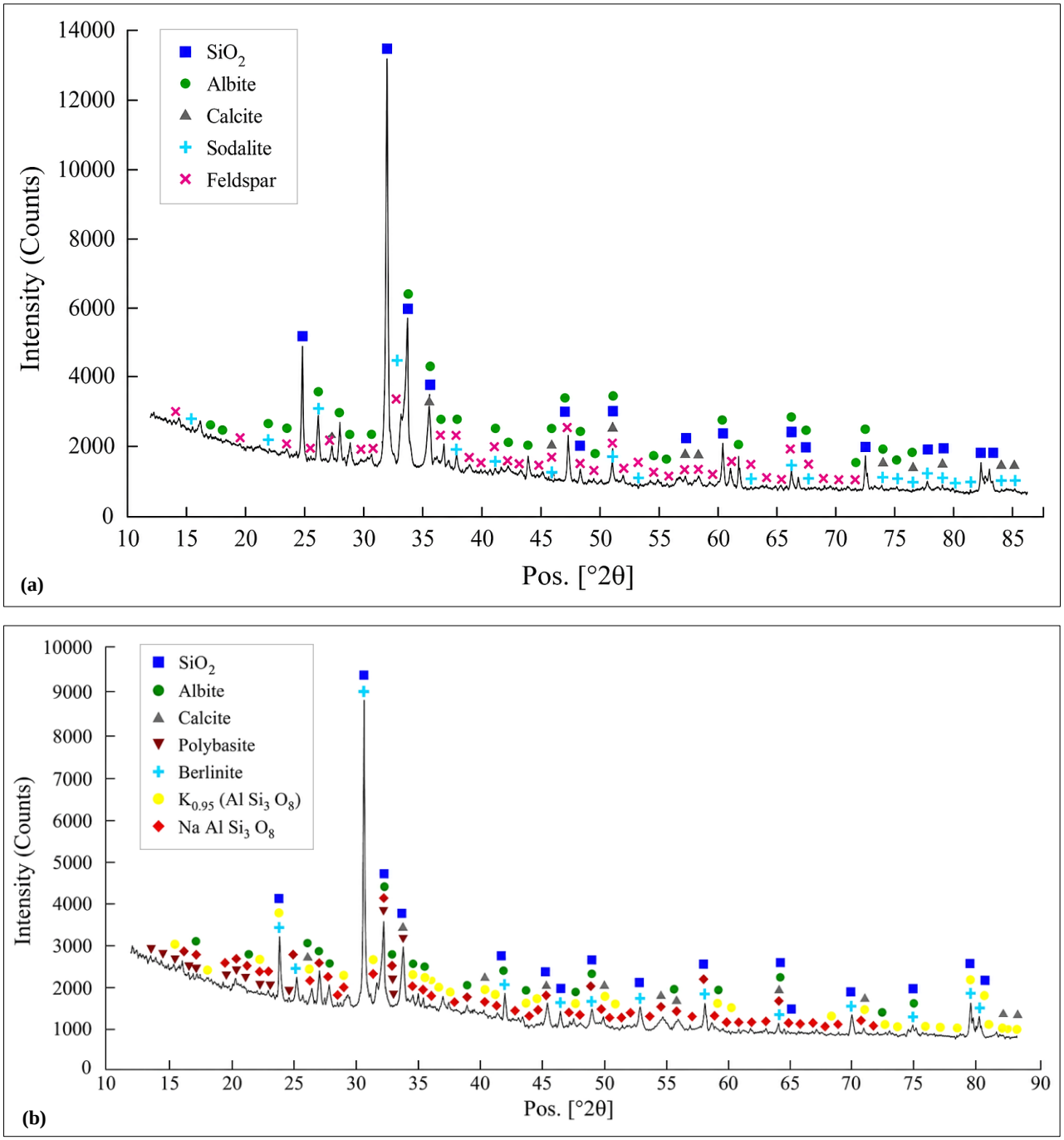

Figure 11. X-ray diffraction patterns of hardened concrete: (a) control mixture and (b) optimal mixture (P4)

3.5.2. Fourier Transform Infrared Spectroscopy (FTIR)

The FTIR spectra of P1 and P4 are compared in Figure 12. FTIR analysis identified characteristic absorption bands in both P1 and P4, with subtle but significant differences reflecting distinct hydration product distributions. The Si–O stretch at 997 cm^{-1} (characteristic of C-S-H silicate networks) appeared more intense in P4 spectra relative to P1, suggesting higher C-S-H polymerization density and more complete hydration of silicate phases. The C=O stretch at 1417 cm^{-1} (carbonation product, calcite) showed comparable intensities between P1 and P4, consistent with similar bulk carbonation depths measured by phenolphthalein testing. The O–H stretch region (3200–3600 cm^{-1}) displayed subtle baseline elevation in P4, indicating higher water content associated with C-S-H gel, a finding consistent with the hypothesis that biopolymer additives promote more hygroscopic hydration product morphologies. The absence of diagnostic bands for unreacted Aloe vera polysaccharides (characteristic C–H stretches around 2900 cm^{-1} would be pronounced) suggests complete consumption of the biopolymer during hydration, likely through complexation with calcium and silicate ions rather than simple physical adsorption.

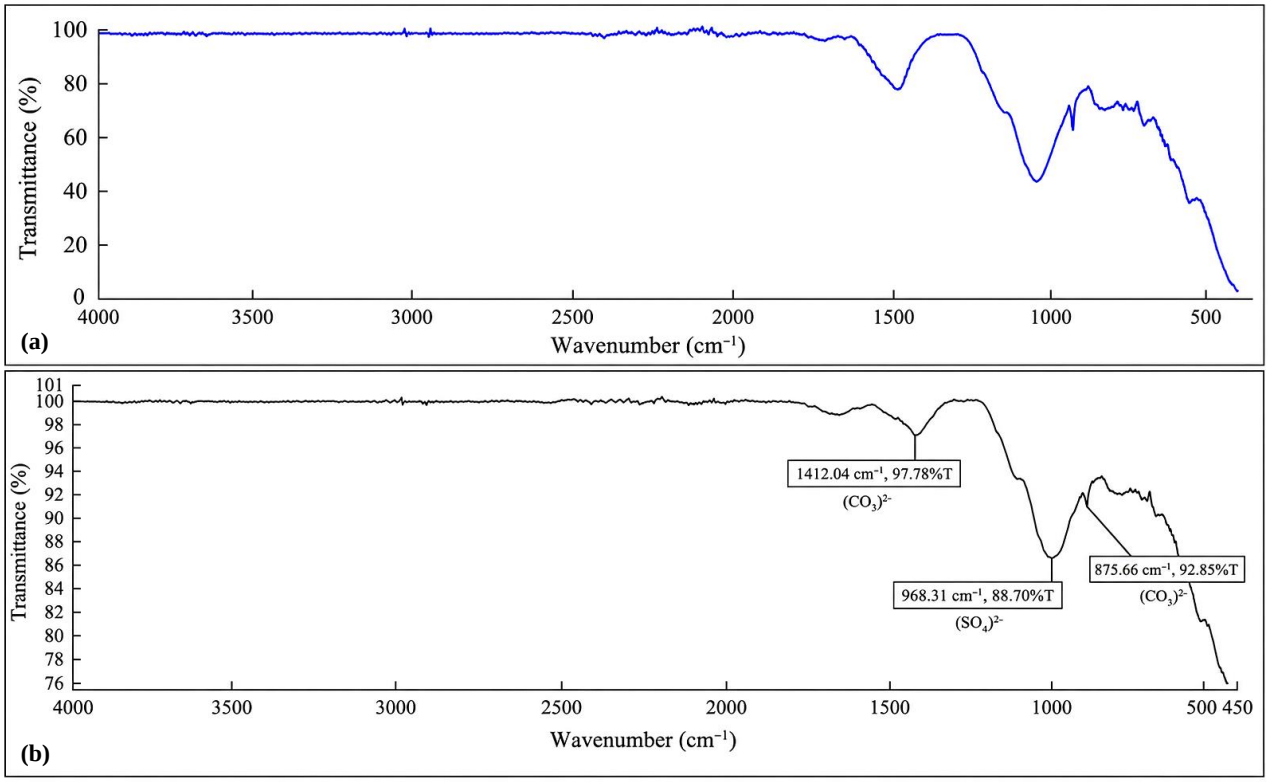

Figure 12. FTIR spectra of the samples: (a) reference material and (b) modified material

3.5.3. Scanning Electron Microscopy (SEM-EDS)

Typical SEM images of the cement paste and ITZ for P1 and P4 are displayed in Figure 13. Microstructural examination by SEM revealed striking morphological differences between P1 and P4. The control mixture (P1) displayed a relatively coarse pore network with well-defined capillary pores (5–50 μm diameter) and visible unreacted cement grains, characteristic of conventional concrete microstructure. The interfacial transition zone (ITZ) between aggregate and paste was clearly demarcated with visible porosity and reduced mineral density.

In contrast, P4 exhibited a refined pore structure with smaller, more uniformly distributed pores (<5 μm typical diameter) and minimal visible porosity. The paste-aggregate interface showed substantially improved mineral contact and reduced interfacial void space, consistent with enhanced ITZ densification. EDS elemental analysis revealed locally elevated carbon content in specific zones of P4, confirming the presence of polysaccharide-derived organic compounds within the microstructure, likely bound to hydration product surfaces through chemical complexation rather than mechanical inclusion. The observed morphological improvements align quantitatively with the measured strength gains (8.9% at 28 days) and permeability reductions (9.7% at 56 days), providing direct microstructural evidence supporting the proposed synergistic mechanism: biopolymer promotion of denser C-S-H formation combined with crystalline waterproofing agent blockage of residual capillary pathways.

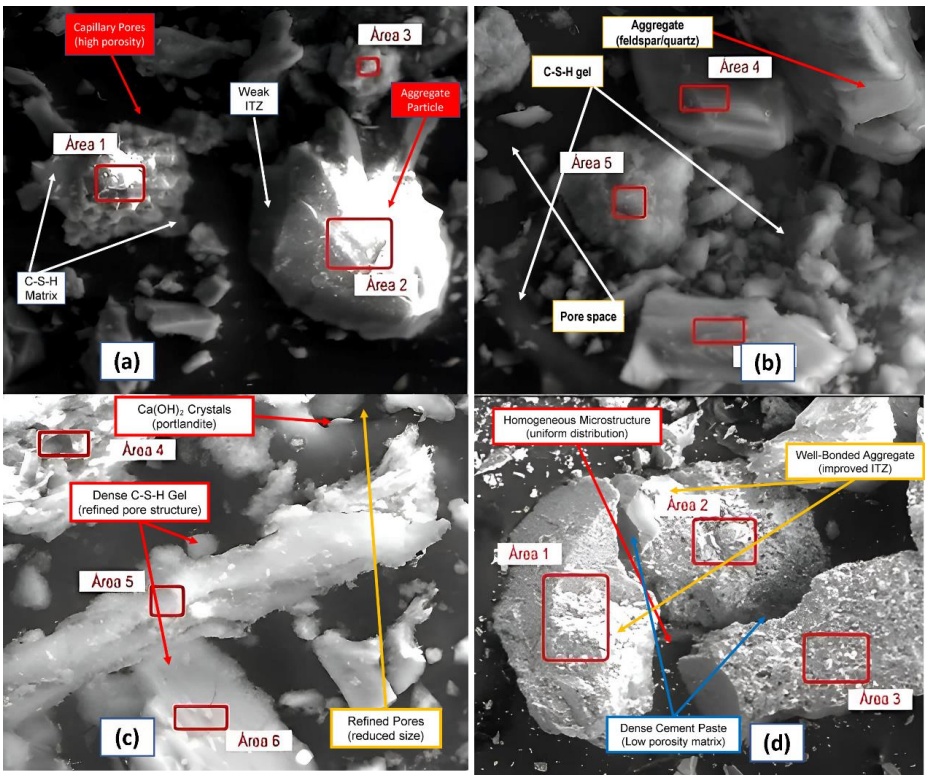

Figure 13. SEM images of the cement paste microstructure and the interfacial transition zone. (a, b) reference sample with high capillary porosity and less dense C-S-H gel, and (c, d) modified sample with dense C-S-H gel, refined pores and better adhered aggregates.

3.6. Structural Behavior of Scaled Frames

The load–displacement and strain responses for the U‑ frame and C‑ frame tests are plotted in Figure 14. The pilot-scale structural testing program validated laboratory-measured strength and stiffness improvements through load-displacement testing of reinforced concrete frames cast with P1 and P4 mixtures. Both frame configurations (inverted U-frame with vertical loading and C-frame with horizontal joint loading) remained elastic up to approximately 60% of design load, with measurable but recoverable deformations. At higher load levels (80–100% design capacity), nonlinear softening behavior emerged, characteristic of reinforced concrete approaching serviceability limits. Strain gauge measurements on longitudinal reinforcement showed that the P4 frame experienced 9.6% lower maximum strain (600.52 microstrain (με) vs. 664.57 με in P1 at final loading step) at identical load levels, confirming improved structural stiffness and reduced deformability in concrete cast with the optimal admixture combination. This behavior is consistent with the measured 8.9% higher compressive strength and supports the hypothesis that microstructural densification translates directly to improved structural performance under realistic loading conditions.

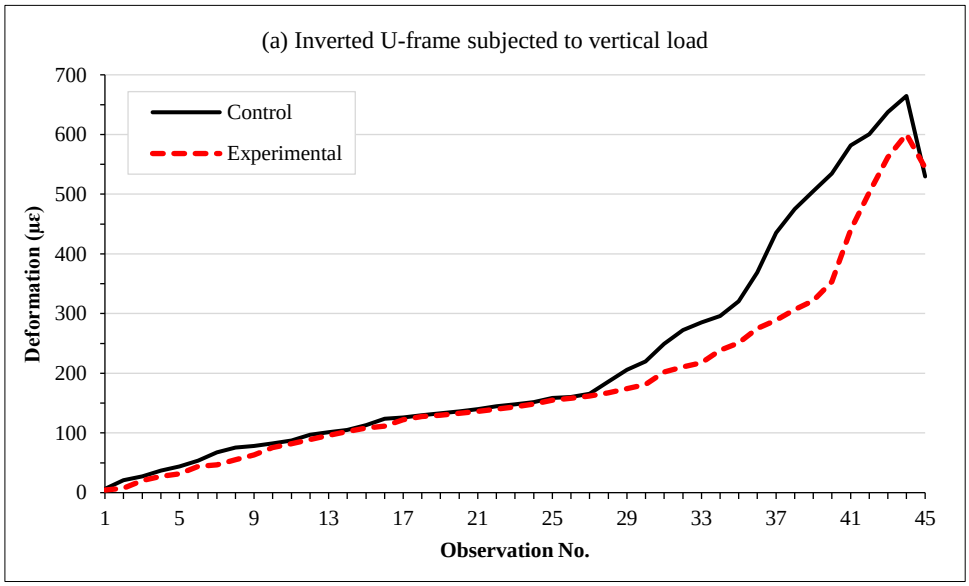

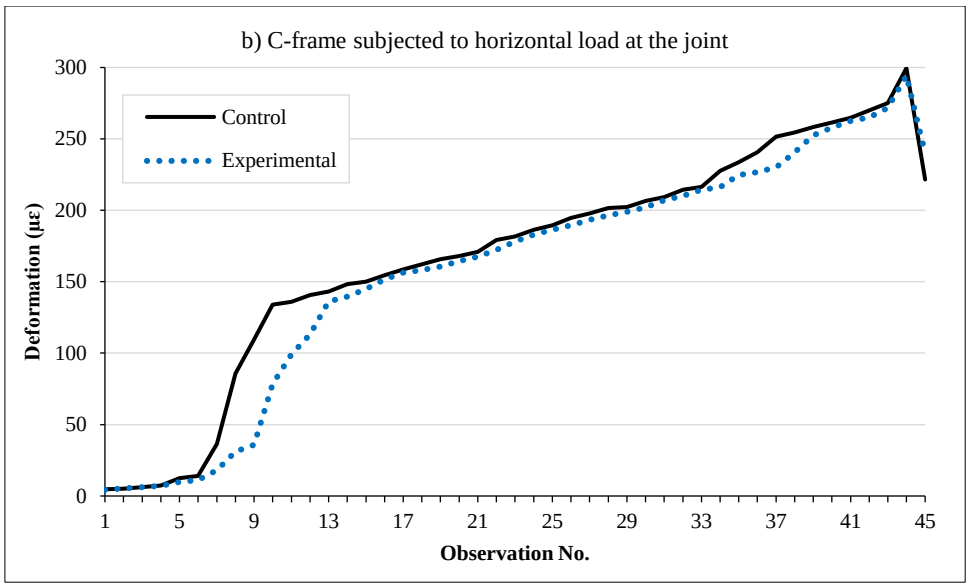

Figure 14. Deformation curves for the standard (P1) and experimental (P4) samples: (a) inverted U-frame subjected to vertical load and (b) C-frame subjected to horizontal load at the joint

3.7. Cost–Benefit Analysis

The main results of the cost–benefit analysis for P1 and P4 are listed in Table 7. The incremental material cost of P4 relative to P1 is 18.24/m³ (USD equivalent $0.60/f³), representing an 11.2% premium. The cost is distributed across S1 (16.34/m³) and AV gel (2.90/m³), with remaining concrete constituents (cement, aggregates, water) held constant. The normalized performance index (P_i) was calculated as a weighted average of mechanical and durability indicators: compressive strength (0.25 weight), flexural strength (0.25 weight), water permeability inverted (0.25 weight), and UPV quality (0.25 weight). P4 achieved P_i = 1.228 relative to control P1 (P_i = 1.000), representing a 22.8% overall performance improvement. The cost-benefit index was calculated as:

$$G_i = \frac{C_0 \times P_{i,P4}}{C_i \times P_{i,P1}} = \frac{162.93 \times 1.228}{181.17 \times 1.000} = 1.104 \quad (6)$$

With G_i = 1.104 > 1.0, the economic analysis demonstrates that P4 delivers 22.8% performance improvement at a cost of only 11.2% material premium, yielding a favorable cost-benefit ratio. Expressed alternatively, P4 provides performance value at 0.149/performance unit compared to 0.195 for the control, representing a 23.6% cost efficiency advantage.

While comprehensive life-cycle cost analysis lies outside the present study's scope, preliminary estimation based on durability improvements suggests substantial long-term economic advantage. The observed reductions in:

- Water permeability (9.7%)
- Chloride penetration (13.7% at 28 days)
- Carbonation depth (24.1%)

collectively extend the time-to-corrosion initiation (T_i) according to the Tuutti model (Equation 7):

$$T_i = \frac{\left(\frac{X_d}{k_c}\right)^2}{D_{app}} \quad (7)$$

where, T_i is time to initiation, X_d is concrete cover thickness, k_c is carbonation coefficient, and D_{app} is apparent chloride diffusion coefficient. For a typical marine structure with 50 mm cover and 50-year service life, a 24% reduction in carbonation rate extends the safe service period by approximately 40%, translating to a conservatively estimated 20-year extension in functional service life.

4. Conclusions

This investigation presents a comprehensive multi-scale evaluation of the synergistic effects of an integral waterproofing admixture (Sika®-1) combined with Aloe vera biopolymer gel on concrete performance across fresh properties, mechanical strength development, durability resistance, microstructural characteristics, pilot-scale structural behavior, and techno-economic viability. The principal findings are summarized as follows:

- Optimal Mixture Composition (P4: 3%S1+2%AV) yielded the most balanced performance improvement across multiple performance metrics, with early-age strength acceleration (12.4% at 7 days, 8.9% at 28 days compressive strength) and superior durability in chloride and carbonation resistance environments.
- Fresh Concrete Behavior remained within practical limits for all formulations (slump 4.0–4.5 inches, air content 1.7–2.7%), demonstrating that the hybrid admixture system does not compromise constructability or placement characteristics. Rheological analysis revealed compensatory interaction between silicate-based pore blockage and biopolymer viscosity modulation, resulting in rheological equilibrium at high admixture dosages.
- Transport Property Improvements were the most pronounced durability benefit, with P4 achieving 9.7% reduced water permeability, 13.7% lower chloride penetration (RCPT at 28 days), and 24.1% reduced carbonation depth at 56 days. These improvements align with extended time-to-corrosion initiation, potentially adding 15–25 years to service life in chloride-rich or carbonation-prone environments.
- Durability Trade-off with Sulfate Exposure was identified: while chloride and carbonation resistance improved substantially, sulfate expansion increased 12.05% in the optimal mixture. This finding underscores the importance of environment-specific admixture selection and suggests that P4 formulation is optimally suited for marine and urban infrastructure but less suitable for arid, industrial, or subsurface applications where sulfate attack dominates.
- Microstructural Validation via XRD, FTIR, and SEM-EDS confirmed that measurable strength and transport property improvements correspond to genuine microstructural densification: refined pore structure (SEM imaging), enhanced C-S-H polymerization (FTIR Si–O band intensification at 997 cm^{-1}), and improved interfacial transition zones (ITZ morphology). These findings provide mechanistic evidence linking microstructure to macroscopic performance improvements.
- Structural-Scale Performance was validated through pilot reinforced concrete frame testing, which demonstrated that laboratory-measured strength gains (8.9% at 28 days) translated to 9.6% reduction in maximum strain under equivalent loading conditions. This finding provides confidence for engineering design applications and real-world deployment.
- Economic viability was established through cost-benefit analysis (index G_i = 1.104), indicating that P4 delivers 22.8% overall performance improvement at an 11.2% material cost premium. Life-cycle cost considerations suggest cost recovery within 10–15 years of service in high-maintenance environments through durability-driven reductions in repair frequency and extent.

4.1. Limitations and Recommendations for Future Research

This research, although exhaustive in scope, has some limitations that require recognition:

- Only four mixing ratios were evaluated. Other mix dosing combinations would detect potential synergistic peaks outside the tested range.
- The unexpected increase in sulfate expansion (12.05% in P4) warrants a detailed investigation using post-exposure ERX to identify phase transformations and suppression mechanisms of ettringite formation.
- Although microstructural evidence supports synergistic interaction, direct molecular-scale characterization of polysaccharide–cement interactions would strengthen the mechanistic understanding.

5. Declarations

5.1. Author Contributions

Conceptualization, M.C.; methodology, M.C., R.S., and L.V.; software, J.G. and B.P.; validation, M.C.; formal analysis, J.G.; investigation, J.G. and B.P.; resources, O.A., J.G., and B.P.; data curation, R.S. and L.V.; writing—original draft preparation, J.G. and B.P.; writing—review and editing, M.C.; visualization, R.S., P.P., O.C., and L.V.; supervision, M.C. and O.A.; project administration, M.C. All authors have read and agreed to the published version of the manuscript.

5.2. Data Availability Statement

The data presented in this study are available upon request from the corresponding author. The data are not publicly available due to ongoing intellectual property considerations related to the optimized hybrid formulation and confidentiality agreements with third-party analytical laboratories.

5.3. Funding

The authors received no financial support for the research, authorship, and/or publication of this article.

5.4. Acknowledgments

We appreciate the support by Cesar Vallejo University during the development of this scientific article. We would also like to thank the experts and peer reviewers for their suggestions and recommendations.

5.5. Conflicts of Interest

The authors declare no conflict of interest.

6. References

[1] Shalchian, M. M., Arabani, M., Farshi, M., Ranjbar, P. Z., Khajeh, A., & Payan, M. (2025). Sustainable construction materials: Application of chitosan biopolymer, rice husk biochar, and hemp fibers in geo-structures. Case Studies in Construction Materials, 22(January), 4528. doi:10.1016/j.cscm.2025.e04528.

[2] Caldas, L. R., de Araujo, A. F., Hasparyk, N. P., Tiecher, F., Amantino, G., & Filho, R. D. T. (2022). Circular economy in concrete production: Greenhouse Gas (GHG) emissions assessment of rice husk bio-concretes. Revista IBRACON de Estruturas e Materiais, 15(6), e15602. doi:10.1590/S1983-41952022000600002.

[3] Chen, L., Huang, L., Hua, J., Chen, Z., Wei, L., Osman, A. I., Fawzy, S., Rooney, D. W., Dong, L., & Yap, P. S. (2023). Green construction for low-carbon cities: a review. Environmental Chemistry Letters, 21(3), 1627–1657. doi:10.1007/s10311-022-01544-4.

[4] Suclupe, R., Cubas, M., Correa, Y., & Maza, J. (2024). Influence of Rice Husk Ash as a Partial Substitute for Cement on the Microstructure and Mechanical Properties of Concrete. Civil Engineering and Architecture, 12(5), 3697–3715. doi:10.13189/cea.2024.120540.

[5] Melendrez Llontop, M. S., Fernández Salazar, V. A., Cubas Armas, M. R., & Suclupe Sandoval, R. E. (2025). Sustainable structural concrete optimization with locust bean pod ash and silica fume: impact on mechanical properties. Innovative Infrastructure Solutions, 10(6), 14. doi:10.1007/s41062-025-02043-5.

[6] Cubas, M., Correa, E., Benavides, W., Suclupe, R., & Arriola, G. (2025). Modified Asphalt Mixtures Incorporating Pulverized Recycled Rubber and Recycled Asphalt Pavement. Civil Engineering Journal (Iran), 11(2), 420–436. doi:10.28991/CEJ-2025-011-02-02.

[7] Stivaros, P. C. (2025). Service life evaluation in concrete rehabilitation – a sustainability benefit. Revista Alconpat, 15(2), 205–217. doi:10.21041/ra.v15i2.814.

[8] Miah, M. J., Miah, M. S., Mughal, H., & Hasan, N. M. S. (2025). Mitigating Environmental Impact Through the Use of Rice Husk Ash in Sustainable Concrete: Experimental Study, Numerical Modelling, and Optimisation. Materials, 18(14), 3298. doi:10.3390/ma18143298.

[9] Kalokhe, P. V., & Kshirsagar, M. P. (2025). Impact of Biopolymers on the Mechanical and Durability Properties of Concrete: A Comprehensive Review. Revue Des Composites et Des Materiaux Avances, 35(5), 909–923. doi:10.18280/rcma.350511.

[10] Ahmed, S., & Memon, F. A. (2022). Experimental study on aloe vera gel as a water reducing admixture in concrete. International Research Journal of Modernization in Engineering Technology and Science, 4(5), 2796-2800.

[11] Vignesh, J., Ramesh, B., & Xavier, J. R. (2025). A review of recent trends in sustainable biopolymer-integrated concrete and its impact on mechanical performance and structural reliability. International Journal of Biological Macromolecules, 321, 146408. doi:10.1016/j.ijbiomac.2025.146408.

[12] Barco-Tocto, E. K., Agüero-Hualcas, D. S., & Farfán-Córdova, M. (2025). Nopal extract and aloe vera to improve structural concrete exposed to saline environments. Revista Facultad de Ingeniería Universidad de Antioquia, (115), 62-74. doi:10.17533/udea.redin.20240514.

[13] Oshim, U. E., Onwuka, D. O., Njoku, F. C., Onwuka, U. S., & Anyaogu, L. (2025). Prediction of flexural strength of concrete containing aloe vera gel as admixture using Ibearugbulem's regression method. UNIZIK Journal of Engineering and Applied Sciences, 4(1), 1504-1516.

[14] Aher, P. D., Patil, Y. D., Waysal, S. M., & Bhoi, A. M. (2023). Critical review on biopolymer composites used in concrete. Materials Today: Proceedings. doi:10.1016/j.matpr.2023.07.212.

[15] Suwondo, R., Suangga, M., Dario, A., & Cunningham, L. (2024). Enhancing Concrete Durability Through Crystalline Waterproofing Admixtures: a Comprehensive Performance Evaluation. International Journal of GEOMATE, 26(114), 17–24. doi:10.21660/2024.114.4074.

[16] Wang, C., Xiao, J., Long, C., Zhang, Q., Shi, J., & Zhang, Z. (2023). Influences of the joint action of sulfate erosion and cementitious capillary crystalline waterproofing materials on the hydration products and properties of cement-based materials: A review. Journal of Building Engineering, 68, 106061. doi:10.1016/j.jobe.2023.106061.

[17] Fang, Y., Wang, Z., Yan, D., Lai, H., Ma, X., Lai, J., Liu, Y., Zhong, L., Chen, Z., Zhang, X., Lin, Z., & Wang, D. (2024). Study on rheological, adsorption and hydration properties of cement slurries incorporated with EPEG-based polycarboxylate superplasticizers. Frontiers in Materials, 11, 1358630. doi:10.3389/fmats.2024.1358630.

[18] Moeinian, M., Ardjmand, M., & Nosratinia, F. (2024). Evaluating the operational properties of concrete admixtures containing molecularly modified polycarboxylate superplasticizers. Scientific Reports, 14(1), 20170. doi:10.1038/s41598-024-71078-y.

[19] Li, W., Wei, Q., Chen, Q., & Jiang, Z. (2022). Effect of CO32- and Ca2+ on self-healing of cementitious materials due to "build-in" carbonation. Journal of Building Engineering, 56, 104781. doi:10.1016/j.jobe.2022.104781.

[20] Gojević, A., Ducman, V., Grubeša, I. N., Baričević, A., & Pečur, I. B. (2021). The effect of crystalline waterproofing admixtures on the self-healing and permeability of concrete. Materials, 14(8), 1860. doi:10.3390/ma14081860.

[21] Zhao, Y., Yang, B., Zhang, K., Guo, A., Yu, Y., & Chen, L. (2025). Machine Learning Models for Predicting Freeze–Thaw Damage of Concrete Under Subzero Temperature Curing Conditions. Materials, 18(12), 2856. doi:10.3390/ma18122856.

[22] Qin, Q., Ma, H., Liang, L., Liu, Y., Lv, Z., Wang, J., & Jin, P. (2024). Effect of heat-treatment on corrosion behavior of Mg-4Gd-2Nd alloy. Journal of Materials Research and Technology, 29, 3156-3167. doi:10.1016/j.jmrt.2024.02.045.

[23] Ševčík, R., Kolář, M., Pokorný, J., Zárybnická, L., Honzíček, J., & Machotová, J. (2025). Polymeric bio-based nanodispersed admixtures for the production of hydrophobic Portland cement mortars. Frontiers in Built Environment, 11, 1701378. doi:10.3389/fbuil.2025.1701378.

[24] Oshim, U. E., Onwuka, D. O., Njoku, F. C., & Onwuka, U. S. (2024). Application of Regression Model in Predicting Compressive Strength of Concrete Incorporating Aloe Vera Gel as Admixture. Journal of Materials Engineering, Structures and Computation, 3(4), 39–53. doi:10.5281/zenodo.14576774.

[25] Liu, C., Cui, Y., Pi, F., Cheng, Y., Guo, Y., & Qian, H. (2019). Extraction, purification, structural characteristics, biological activities and pharmacological applications of acemannan, a polysaccharide from aloe vera: A review. Molecules, 24(8), 1554. doi:10.3390/molecules24081554.

[26] SIKA WT-240P. (2019). Crystalline Waterproofing Admixture. SIKA USA, New Jersey, United States. Available online: https://usa.sika.com/en/construction/concrete/contact-us/crystalline-waterproofing-admixture.html (accessed on April 2026).

[27] Wang, Y., Wang, W., & Wang, L. (2022). Understanding the relationships between rheology and chemistry of asphalt binders: A review. Construction and Building Materials, 329. doi:10.1016/j.conbuildmat.2022.127161.

[28] Palacios, M., Flatt, R. J., Puertas, F., & Sanchez-Herencia, A. (2012). Compatibility between polycarboxylate and viscosity-modifying admixtures in cement pastes. American Concrete Institute, ACI Special Publication, 288 SP, 29–42. doi:10.14359/51684218.

[29] Liu, B., Wang, S., Jia, W., Ying, H., Lu, Z., & Hong, Z. (2024). The Effect of RHA as a Supplementary Cementitious Material on the Performance of PCM Aggregate Concrete. Buildings, 14(7), 2150. doi:10.3390/buildings14072150.

[30] Andrade Neto, J. da S., de França, M. J. S., Amorim Júnior, N. S. de, & Ribeiro, D. V. (2021). Effects of adding sugarcane bagasse ash on the properties and durability of concrete. Construction and Building Materials, 266, 120959. doi:10.1016/j.conbuildmat.2020.120959.

[31] Antolín-Rodríguez, A., Merino-Maldonado, D., Fernández-Raga, M., González-Domínguez, J. M., Morán-del Pozo, J. M., Pozo, M. del, García-González, J., & Juan-Valdés, A. (2024). Microstructural, durability and colorimetric properties of concrete coated with a controlled application of graphene oxide. Journal of Building Engineering, 86(December), 108920. doi:10.1016/j.jobe.2024.108920.

[32] Pang, J., Guo, J., Li, W., & Chang, Q. (2023). Effect of chain transfer agents in polycarboxylate superplasticizer on slump-retention of concrete. Canadian Journal of Chemical Engineering, 101(12), 6919–6927. doi:10.1002/cjce.25017.

[33] Hu, M., Ji, S., Sun, Y., & Zhu, K. (2025). Understanding the low-temperature fracture behavior of rejuvenated high viscosity modified asphalt utilizing a combined microstructure-component analysis. Construction and Building Materials, 471(2), 140717. doi:10.1016/j.conbuildmat.2025.140717.

[34] Minjares-Fuentes, R., Femenia, A., Comas-Serra, F., & Rodríguez-González, V. M. (2018). Compositional and structural features of the main bioactive polysaccharides present in the aloe vera plant. Journal of AOAC International, 101(6), 1711–1719. doi:10.5740/jaoacint.18-0119.

[35] Yu, Z., Wang, Y., & Li, J. (2022). Performance Investigation and Cost–Benefit Analysis of Recycled Tire Polymer Fiber-Reinforced Cemented Paste Backfill. Polymers, 14(4), 708. doi:10.3390/polym14040708.

[36] dos Santos Lima, G. T., Oliveira, M. V. C., de Andrade Pinto, R. C., & Rocha, J. C. (2023). Is the diffuse ultrasound method reliable for evaluating autonomous self-healing in cementitious materials with expansive agent pellets?. Materials Letters, 351, 135058. doi:10.1016/j.matlet.2023.135058.

[37] Aranda Cuevas, B., Herrera Méndez, C. H., Flores, I. I., Solís-Pereira, S., Cuevas-Glory, L., Muñoz, G. R., Vargas y Vargas, M. de L., & Cortez, J. T. (2016). Main Polysaccharides Isolated and Quantified of Aloe vera Gel in Different Seasons of the Year. Food and Nutrition Sciences, 07(06), 447–453. doi:10.4236/fns.2016.76046.

[38] Aburto-Moreno, Z., Alvarado-Quintana, H., & Vásquez-Alfaro, I. (2018). Influence of the percentage of aloe-vera on compressive strength, infiltration, capillary absorption, time of setting and settlement in a structural concrete. Sciéndo, 21(2), 105–118. doi:10.17268/sciendo.2018.011.

[39] Yehia, S., Ibrahim, A. M., & Ahmed, D. F. (2023). The impact of using natural waste biopolymer cement on the properties of traditional/fibrous concrete. Innovative Infrastructure Solutions, 8(11), 287. doi:10.1007/s41062-023-01253-z.

[40] Zhang, Z., Zhang, D., Zhou, J., Zhang, D., & Tan, K. H. (2025). A critical review on high temperature performance of sustainable cementitious materials. Npj Materials Sustainability, 3(1). doi:10.1038/s44296-025-00081-9.

[41] Polat, R., Demirboğa, R., Karakoç, M. B., & Türkmen, İ. (2010). The influence of lightweight aggregate on the physico-mechanical properties of concrete exposed to freeze–thaw cycles. Cold Regions Science and Technology, 60(1), 51-56. doi:10.1016/j.coldregions.2009.08.010.

[42] Abdellatief, M., Hassan, Y. M., Elnabwy, M. T., Wong, L. S., Chin, R. J., & Mo, K. H. (2024). Investigation of machine learning models in predicting compressive strength for ultra-high-performance geopolymer concrete: A comparative study. Construction and Building Materials, 436, 136884. doi:10.1016/j.conbuildmat.2024.136884.

[43] Mousavinezhad, S., Toledo, W. K., Newtson, C. M., & Aguayo, F. (2024). Rapid Assessment of Sulfate Resistance in Mortar and Concrete. Materials, 17(19), 4678. doi:10.3390/ma17194678.